UW-Madison.
SSEC Publication No.98.02.C1.

Space Science and Engineering Center
University of Wisconsin–Madison

Measurement Studies for Defining NPOESS Requirements and NAST Algorithm Development

A REPORT from the

COOPERATIVE INSTITUTE FOR METEOROLOGICAL SATELLITE STUDIES

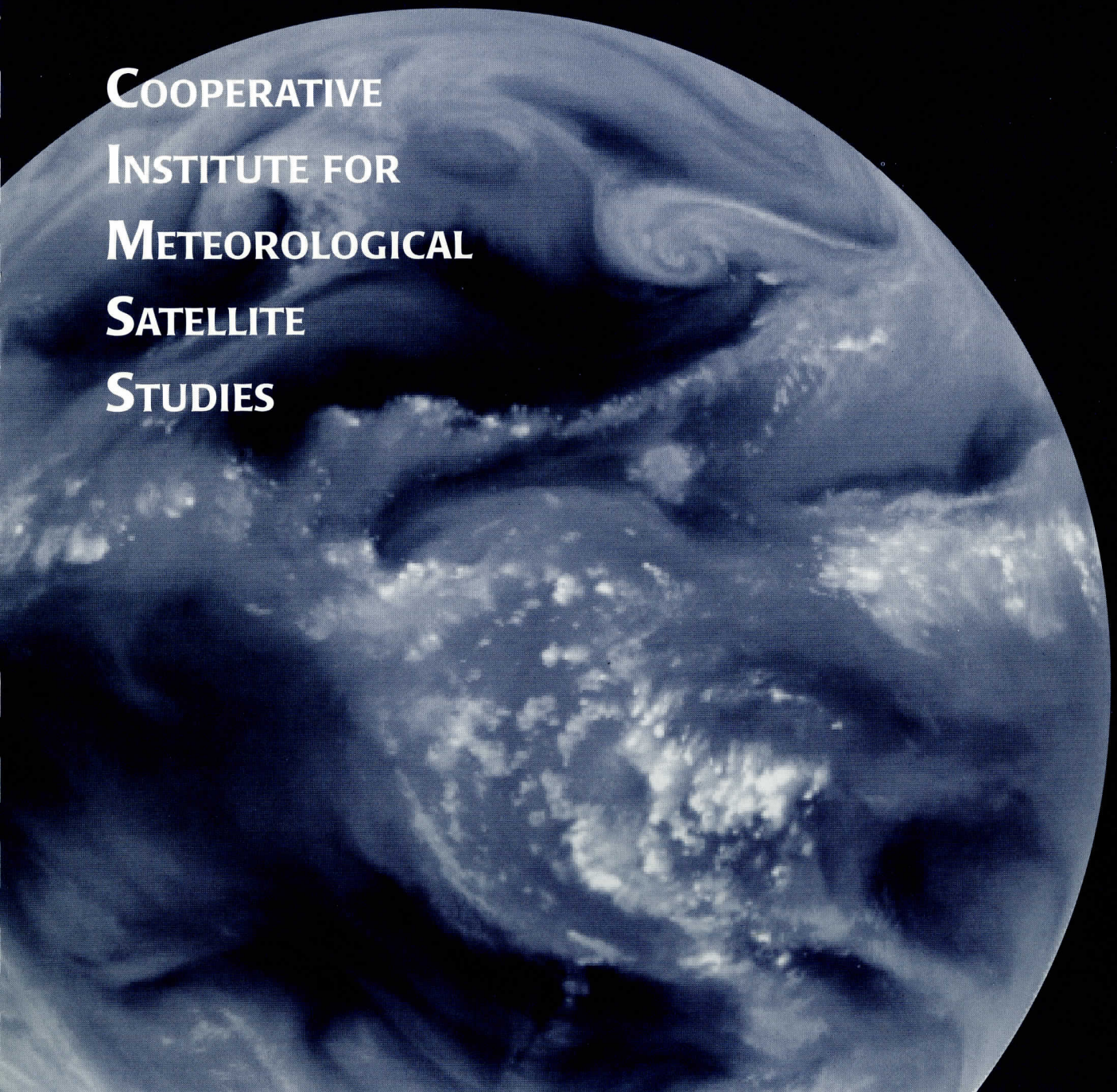

THE SCHWERDTFEGER LIBRARY
1225 W. Dayton Street
Madison, WI 53706

Measurement Studies for Defining NPOESS Requirements and NAST Algorithm Development

Cooperative Institute for Meteorological Satellite Studies
University of Wisconsin-Madison
1225 West Dayton Street
Madison, WI. 53706

February 1998

Table of Contents

1.0 Introduction

The intent of this study is focused primarily on sounding the atmosphere in the presence of clouds and defining suitable instrument options necessary to fulfill this objective. Since simulations which include atmospheric clouds are constrained under some circumstances, this current study will implement the use of new and existing data from the latest ER-2 remote sensing instruments to offset the limitations imposed by model simulations; therefore, real data is currently being used to evaluate the trade-offs between field of view size and instrument noise which dictates the sounding coverage and accuracy. The High spectral resolution Interferometer Sounder (HIS), Moderate resolution Imaging Spectrometer Airborne Simulator (MAS), and Cloud Lidar System (CLS) are the main ER-2 instrument data sources used in this study for defining the field of view and noise criteria. Spatial averaging of cloudy and clear observations from HIS data are used to simulate the spatial sampling and spatial characteristics of the advanced sounding instruments proposed for (National Polar-orbiting Operational Environmental Satellite System) NPOESS. HIS, MAS, and CLS each provide useful data for evaluating cloudy sounding methods through integrated usage and provide better spatial and spectral coverage which is necessary in defining the requirements for the NPOESS Atmospheric Sounding Testbed (NAST). These key areas are crucial in the defining the best optimization of the CrIS observing characteristics and for evaluating the instrument options necessary for an advanced Interferometer Thermal Sounder (ITS). Results from this two year study will indicate which trade-offs are necessary to balance the technical demands required to provide accurate soundings of the atmosphere under partly cloudy and clear conditions. This review will present work completed to date and outline the future work needed to properly define the NAST / NPOESS requirements.

2.0 Overview

2.1 Background

The design concept of the Interferometer Thermal Sounder (ITS) specifies that the design be practical for sounding radiance data within the constraints imposed by the NPOESS system. These constraints on size, weight, power and data handling of the ITS should not significantly impact the high spectral resolution required to perform accurate atmospheric soundings under varied atmospheric conditions. Since engineering constraints and measurement requirements may conflict under some circumstances, the NAST strategy requires comprehensive studies into the optimal instrument combination to satisfy measurement accuracy and instrument specifications. Sensor field of view changes are a major instrument issue which reflect changes in signal-to-noise, so any decrease in the field of view of the instrument reflects a decrease in the signal-to-noise of the instrument which is normally a linear characteristic. Cloud statistics performed by Smith et al. (1996), Cuomo et al. (1992), and Derrien (1992) have shown that sampling clear fields of view in a broken cloud cover region reveals that both the clear probability sampling and increased instrument resolution increase linearly. Furthermore, an increase in the number of spatially independent measurements does increase the probability of clear air samples within a broken cloud cover region (Smith et al., 1996 and Lee, 1993).

The conflict between measurement accuracy required for obtaining meaningful temperature and water vapor measurements obtained from radiometric data, and field of view requirements needed to maximize the sampling probability within a broken cloud cover area stipulates that specific instrument changes be implemented into the ITS. These fundamental changes in the ITS such as 1) increasing signal-to-noise by cooling the interferometer to cooler temperatures, 2) using a larger aperture area, or 3) increasing the number of detectors can compensate for noise degradation and offset signal-to-noise issues needed to properly obtain valuable radiance measurements from areas with broken cloud cover. The best scenario in achieving the clear air sampling while maintaining the signal to noise is by increasing the number of detectors for the sought after resolution. Cloud statistics from Smith et al. (1996) investigated the probability of obtaining a single clear air sampling within broken to overcast scenes for a 64 linear km area based on resolution and total percentage of clear air samplings for five different scan geometries. Table 1 summarizes the findings of Smith et al. (1996).

resolution (km)	3x3 Box	2x2 Box	Contiguous	1/2 FOV Gap (under sampling)	1/2 FOV Overlap (alias-free sampling)
32	0 %	16 %	17 %	8 %	19 %
16	46 %	35 %	50 %	46 %	54 %
12	56 %	43 %	62 %	60 %	70 %
8	64 %	52 %	71 %	71 %	74 %
4	72 %	63 %	82 %	--	--

Table 1. Probability of finding a single clear field of view for those having a linear dimension of 4, 8, 12, 16, and 32 km field of view within a 64 x 64 km area for broken or overcast cloud cover. The results are based on five scan geometry: 1) 3x3 box array, 2) 2x2 box array, 3) contiguous (nonoverlapping), 4) 50% gap between each field of view (undersampled), and 5) 50% overlap of field of views (alias-free sampling). Results are for January through May 1993 from Smith et al. (1996).

Results from Smith et al. (1996) are consistent with the findings presented by Derrien (1992) and Cuomo et al. (1992) which show that reducing the FOV size for a fixed number of footprints achieves nearly double the amount of clear fields of view.

The use of large detector arrays in lieu of better resolution will maintain the signal-to-noise while increasing the clear air sampling rate of an ITS system. In order to achieve 1 km resolution, 576 detectors or a 24 x 24 detector array would be needed to maintain the signal-to-noise equivalent to 8 km resolution using 9 detectors or a 3 x 3 detector array. The Atmospheric Infrared Sounder (AIRS) instrument set to fly on the EOS-PM platform uses 4,700 detectors, so the concept of using large detector arrays is certainly feasible for atmospheric sounding instruments.

The use of such large detector arrays does require that on board processing be done in order to keep the data transmission rate at a nominal level. Data processing such as performing Fast Fourier Transforms of the interferograms, spectral radiance calibration, and single pixel processing within the ITS field of view used to obtain radiance spatial averages for clear, partly cloudy, or overcast conditions are appropriate on board processing functions. Statistical processing is already done on the ground as a first step in the retrieval process. Categorizing multi-spectral scene data for use in developing cloud masks from aircraft sensors (MAS) and from satellite platforms such as GOES, AVHRR, and HIRS instruments also provide valuable scene information required while performing statistical operations. Figure 1 is an example of a MAS cloud mask which shows that multi-spectral scene data is an integral component for determining a cloud scene at high spatial resolution. For an ITS field of view resolution of 8 km, 64 pieces of cloud obstructed or cloud unobstructed information are available.

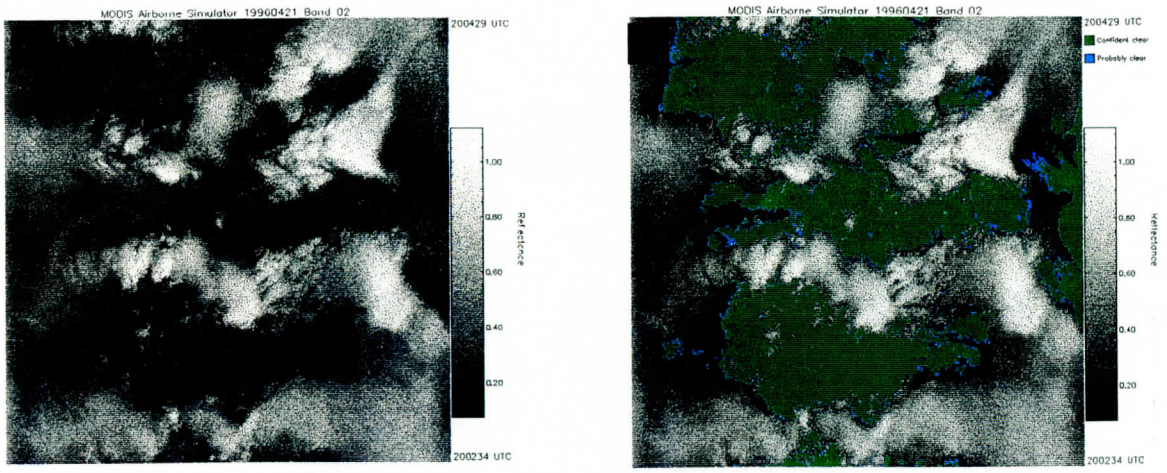

Figure 1. Image (A) is a MAS visible image (0.66 μm) of stratocumulus and altocumulus. Image (B) is the same MAS visible image with MAS cloud mask confident clear air (green) and probably clear air (blue). Image area is 37.25 km x 37.25 km taken from ER-2 aircraft altitude of 20 km. Resolution of the MAS visible image and cloud mask product is 50 meters.

The cloud mask in figure 1 effectively provides a method of registering those areas which are clear with a resolution of 50 meters from an altitude of 20 km. The use of the MAS cloud mask results along with variable ITS field of view resolutions will provide additional statistics on obtaining a clear field of view within a 37.25 km x 67.25 km area covered by MAS data - equivalent to an AMSU footprint. The MAS cloud mask algorithm provides 50 meter resolution detail on obstructed or unobstructed fields of view which allows for a computation of the cloud fraction within an ITS field of view. A high degree of cloud discrimination can be applied to each chosen ITS resolution where such cloud statistic studies were not possible in the past.

The sounding accuracy which can be gained through use of detector arrays of variable dimension within the ITS field of view is currently being addressed using real data and simulations. This report will outline those areas which are currently underway and outline the course of action to be taken over the next year. The next section, briefly outlines the strategy required to meet those objectives necessary to define an operational ITS instrument complement which equally balances the technological requirements with the scientific requirements needed retrieve atmospheric soundings under cloudy conditions.

2.2 Objectives

The objectives include addressing the trade-off between field-of-view size and noise level which are critical components in evaluating instrument options needed for

an optimal instrument configuration necessary to retrieve an atmospheric profile under cloudy conditions. Five specific tasks will be used to accomplish this primary objective:

1. Development of a sampling strategy for optimizing retrievals under partly cloudy conditions.
2. Data sets are used for evaluation of sounder sampling strategies in the presence of clouds.
3. Clear and cloudy retrieval performance analysis.
4. Studies using IMG interferometer data from the Advanced Earth Observing Satellite (ADEOS).
5. NAST scientific Algorithm development.

Task 1, development of a sampling strategy for optimizing retrievals under partly cloudy conditions, will make use of MAS data to study the clear and cloudy probability for variable ITS sounder field of view resolutions. Figure 2 depicts combined MAS

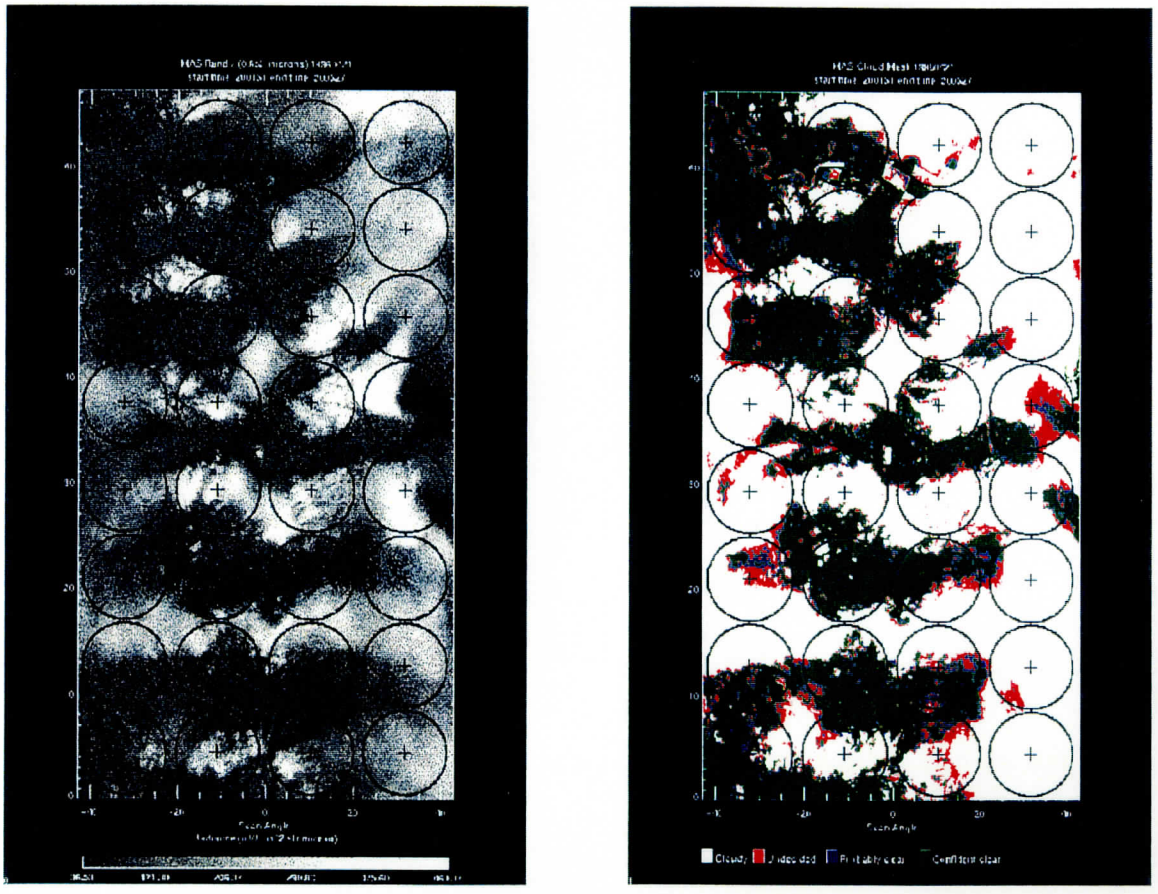

Figure 2. Image (A) is a MAS visible (0.66 μm) image shown in radiance units (mW / m^2 str μm) of stratocumulus and cirrus over Oklahoma during SUCCESS (April 21, 1996). Image (B) is the cloud mask algorithm solution with 8 km sounder footprint overlays. The area of each image is equivalent to an AMSU footprint - 37.25 km x 67.25 km. Axes are denoted in terms of scan angle (x axis) and kilometers (y axis).

imagery and cloud mask algorithm results that will be used to generate clear and cloudy statistic probabilities. These clear and cloudy probabilities will be based on a 50 km linear resolution sounding area of an AMSU footprint. Figure 2 is an example of using the MAS cloud mask algorithm for computing the cloud / clear statistics for an AMSU footprint on the size order of the MAS and cloud mask images.

Task 2, data sets for evaluation of sounder sampling strategies in the presence of clouds, makes use of data sets from recent field campaigns - SUCCESS (April - May 1996) and WINCE (January - February 1997). HIS observations of clear and cloudy sky conditions are used to simulate real cloud contaminated radiance data for various spatial resolutions and spatial sampling strategies. All cloud clearing techniques are to be validated against the observed 2 km clear sky radiance spectra. MAS data and CLS data will also provide supplementary information on the cloud scene within each simulated ITS field of view and provide additional validation of the cloud clearing techniques.

Task 3, clear and cloudy retrieval performance analysis, constitutes the main performance validation of three retrieval methodologies, clear hole hunting, cloud clearing (N*), and direct simultaneous retrievals. The three retrieval methods will be applied to ITS, AMSU, and MHS data which is simulated from HIS and NAST data accomplished in Task 2. The retrieval methods applied to the different field of view sizes will help to specify an optimal configuration needed to obtain the best CrIS spatial resolution based on technical and scientific requirements.

Task 4, studies using IMG data from ADEOS, will use the IMG interferometer spectrometer data collected from a space based platform. The broad spectral coverage and high spectral resolution of IMG provides a large data set of earth / atmosphere emission observations that will provide calibration studies, forward model validation and atmospheric / surface property retrievals. Validation of the observations obtained from IMG with selected ground truth sites should provide sufficient information needed for meeting NAST.

Task 5, NAST scientific algorithm development, will provide the necessary software processing required for obtaining atmospheric products from infrared and microwave data from NAST. Proven retrieval methods used on HIS and MIR data will be used on the NAST data, and the atmospheric products obtained from NAST will be at 2 km resolution. NAST data is expected to be available by early 1998 and retrieval processing will commence upon receipt of these data sets.

3.0 Methodology

3.1 Development of a sampling strategy for optimizing retrievals under partly cloudy conditions.

The use of MAS data and the MAS cloud mask algorithm to further study the clear / cloudy probability for a variable ITS field of view will commence in year two of this research. Development and refinements to the MAS cloud mask algorithm are nearly complete, and delivery of the level-1B calibrated data from several field campaigns will shortly be made available. The use of the cloud mask algorithm will focus on generation of clear / cloudy statistics for different field of view resolutions and sampling densities, and will encompass large data sets from several field campaigns: ARMCAS (April 1995), SCAR-B (August - September 1995), SUCCESS (April - May 1996), and WINCE (January - February 1997). Figure 11 depicts the achieved number of clear fields and cloud cleared fields of view weighted by (1-N*) using combined HIS and MAS data. Spectral averaging of HIS observations are made to simulate the

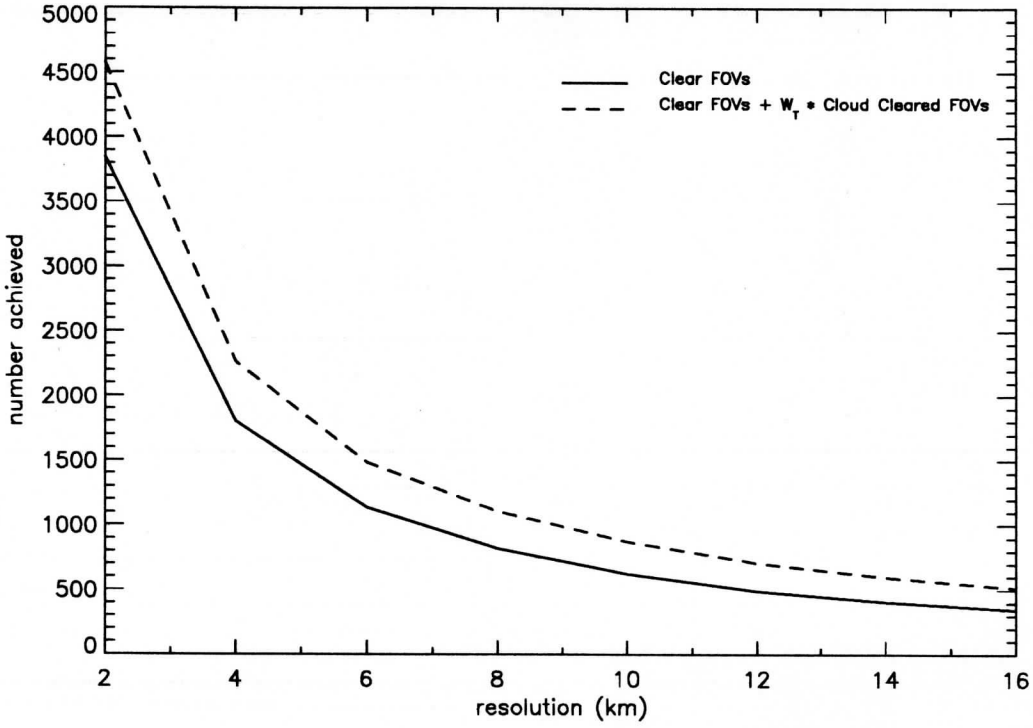

Figure 3. Plot of the number of clear fields of view and cloud cleared fields of view weighted by (1-N*) as a function of spatial resolution for the same area coverage. Spatial resolution is simulated by averaging HIS 2 km footprints and fields of view are determined as either clear or cloudy by the MAS cloud mask within each respective footprint. Eleven days of HIS and MAS data from SUCCESS (April-May 1996) were used in this study.

the differing resolutions sizes, and the MAS cloud mask algorithm is used the determine whether the sounder fields of view are clouded or clear. Clouded fields of view are cleared using the N* method, discussed later, and weighted according to the N* value. Figure 3 shows an exponential decay in the number of clear and weighted cloud cleared fields of view achieved for a nadir viewing sounder used to simulate differing spatial resolutions.

The effect of increased detector noise in the clear air sounding radiance data upon the retrieval accuracy as a function of increasing the field of view size will be accomplished in year two. CLS data will be used to define clear HIS fields of view, and the HIS spectra, will be spatially averaged along a 90 km track - NPOESS sounding area of 40 km x 90 km. The spatially averaged spectra will then be used to obtain temperature and water vapor profiles computed from a full non-linear physical retrieval algorithm. These HIS spectra / retrieved profiles will then be used as the "true" clear and noise free based measurements. Next, artificial detector noise will be added to the "true" clear measurements to simulate the noise imposed upon an ITS as a function of detector field of view. Using a random number generator to simulate the noise effects and the MAS clear air statistics, the "true" clear air spectrum can be defined by the following relation:

$$\varepsilon(d) = \frac{d_0}{d} \frac{\varepsilon(d_0)}{\sqrt{N_{clr}}} \qquad (1)$$

where d is the linear dimension of the field of view (km), N_{clr} is the number of clear fields of view determined from the cloud mask algorithm within the sounding area (MAS 40 km x 90 km viewing area), and $\varepsilon(d_0)$ is the ITS design noise for d_0 the spatial resolution. Retrievals will then be performed on these noise induced radiances and compared against the "true" clear area retrievals for the purpose of defining the relationship between the added noise and the retrieval errors. These differences in retrieval errors between the noise induced spectrum and the "true" spectrum will show the trade-off between detector field of view size and the signal-to noise response.

3.2 Data sets for evaluation of sounder sampling strategies in the presence of clouds.

HIS measurements of the upwelling radiance spectrum, 3.8 μm to 16.8 μm, at 2 km resolution are used to explore possible ways to achieve these measurements under clouded conditions. The objective of this task is to define the degradation upon the sounding accuracy under cloudy sky conditions. The optimal situation is to retrieve

temperature and water vapor information from clear fields of view; however, dynamic weather areas consistently have broken to overcast clouds present. The degradation of this retrieval process is also a function of the ITS instrument design characteristics, so it is important to examine real measurement data which have clouds present within the field of view. When options of using a clear field of view are not available, it becomes important to employ techniques used to separate the cloud radiance spectra from the entire spectra in order to obtain a cloud cleared radiance spectra. The cloud cleared radiance spectra can then be used in the retrieval process. By using the real spatially averaged data with actual cloud conditions, the cloud clearing technique can be simulated using this data under those conditions that would be encountered by the different sounding instrument options proposed to fly on NPOESS.

The cloud clearing technique, often referred to as the N* technique, developed by Smith (1968) and further defined by Chahine (1974) is applied to this specific cloud clearing task. The technique uses two adjacent fields of view with different cloud fraction amounts and a local clear field of view radiance measurement to reconstruct a "declouded" radiance spectrum. By definition, the field of view cloud fraction amount is represented by the following relationship:

$$F = \frac{R_v - R_v^{clr}}{R_v^{cld} - R_v^{clr}} \qquad (2)$$

where F is the fractional cloud cover, R_v is the observed spectral radiance, R_v^{clr} is the clear air radiance and R_v^{cld} is the uniform cloud radiance. The cloud fraction ratio N* is defined as:

$$N^* = \frac{F(S_i)}{F(S_j)} \qquad (3)$$

where s_i and s_j are the geographical positions of the two fields of view. The cloud cleared radiance can be obtained by combining equations (2) and (3) and is represented by the following equation:

$$R_v^{clr} = \frac{R_v(s_i) - N^* R_v(s_j)}{(1 - N^*)} \qquad (4)$$

which yields a radiance spectrum without the observed cloud radiances. The HIS radiance measurements in the presence of clouds will be used to generate cloud cleared radiance results using the N* method for different spatial resolutions, thereby

simulating the type of data achieved by an instrument possessing the different field of view sizes.

These radiance data sets will be produced for different spatial resolutions and sampling characteristics from HIS data collected during SUCCESS and WINCE. The HIS spatial resolution at 20 km is 2 km in the across track direction and 2 km in the along track direction and the radiance measurements are available along the nadir viewing angle. MAS data, which provides high spatial resolution imagery at a resolution of 50 meters, and CLS data will provide the ground truth for the various cloud conditions within each HIS field of view. The heterogeneity of clouds for each flight track can be summarily identified using the MAS imagery and the height of the clouds discerned from CLS Lidar data. Since HIS is a nadir viewing instrument and the proposed ITS will scan along an across track direction, it is necessary to sample along a 180 km linear flight track in order to approximate the density of observations achieved by an across track scanning satellite instrument. The HIS spectra will be averaged over several linear resolutions: 4 km, 8 km, and 16 km. The data sets produced from this study should adequately simulate an instrument which possess the different sized fields of view mentioned above.

Supplementary information provided by CLS and MAS are essential guidance into the type of cloud scene being viewed. CLS determines cloud height information and MAS data provides 50 channels of high spatial resolution imaging across the flight track of the ER-2 flight path. First, CLS is used to define the height of the cloud cover at the nadir viewing angle. Figure 4 cites two examples of CLS determination of the cloud height and also provides additional information on the heights of other cloud layers. The CLS data is used to determine single or multi-level cloud decks within the scene which is necessary when determining optimal conditions for which to apply single layer and uniform cloud clearing techniques. Figure 4 shows multi-level clouds are sporadic in the 960420 case and the 960426 case mainly indicates a single cloud layer persists over the area. Due to the sparse coverage of the CLS data, this study uses the cloud height and cloud layer information provided from the data to determine if the cloud scene is uniform and single layered. Use of the CLS data to determine cloud free scenes are used when available; however, due to the scarcity of the data, the MAS cloud mask algorithm is used to help define clear or clouded sounder or sounder simulated fields of view.

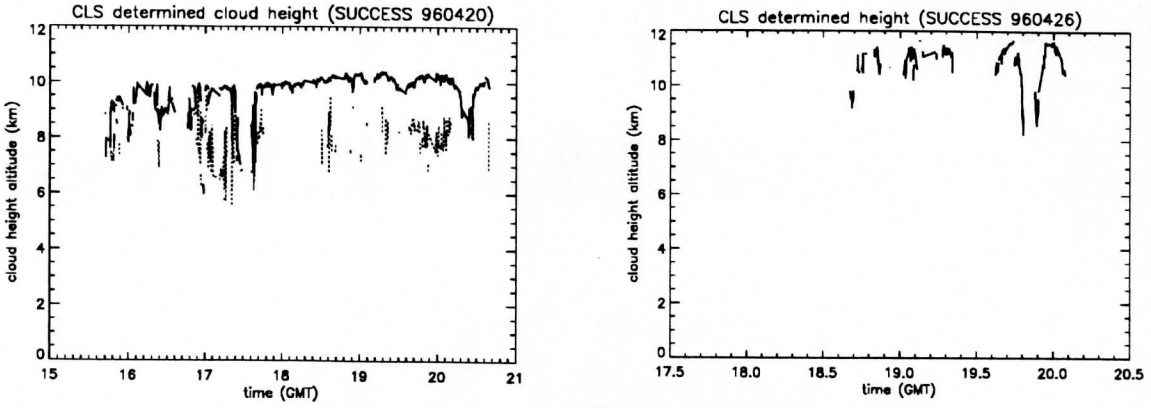

Figure 4. Cloud height determined from Cloud Lidar System from an altitude of 20 km. Solid line represents the uppermost top of the cloud and dashed line represents the second layer of the cloud. The two examples provided are from the SUCCESS field campaign.

Preliminary work using the N* approach in cloud clearing was performed on the 960420 and 960426 cases to evaluate criteria needed to increase the success rate of the N* cloud clearing technique. Figure 5 shows a local clear 2 km resolution HIS radiance spectra measurement for the wavenumbers between 650 to 1050 cm^{-1} (15.4μm to 9.5μm) within a 180 km strip of ER-2 flight path. This clear spectra

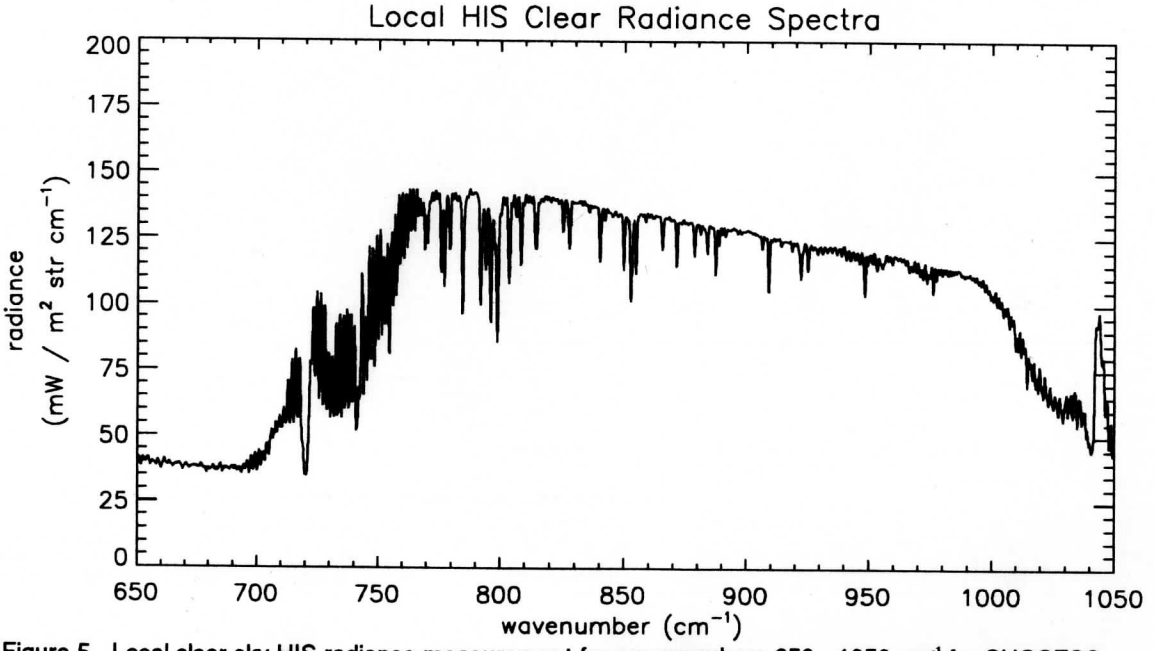

Figure 5. Local clear sky HIS radiance measurement for wavenumbers 650 - 1050 cm^{-1} for SUCCESS case 960420. The spatial resolution of the field of view measurement is 2 km.

used two adjacent 2 km resolution HIS radiance measurements, figure 6, to compute the cloud fraction ratio N* which is crucial in "declouding" the radiance measurements. Each spectra in figure 6 depicts low radiance values which are associated with the HIS

instrument viewing a cloud scene portion within each respective field of view. CLS data indicated the top of the cloud layer at an altitude of 9,175 meters above ground level and MAS imagery verifies the cloud type is predominately composed of cirrus.

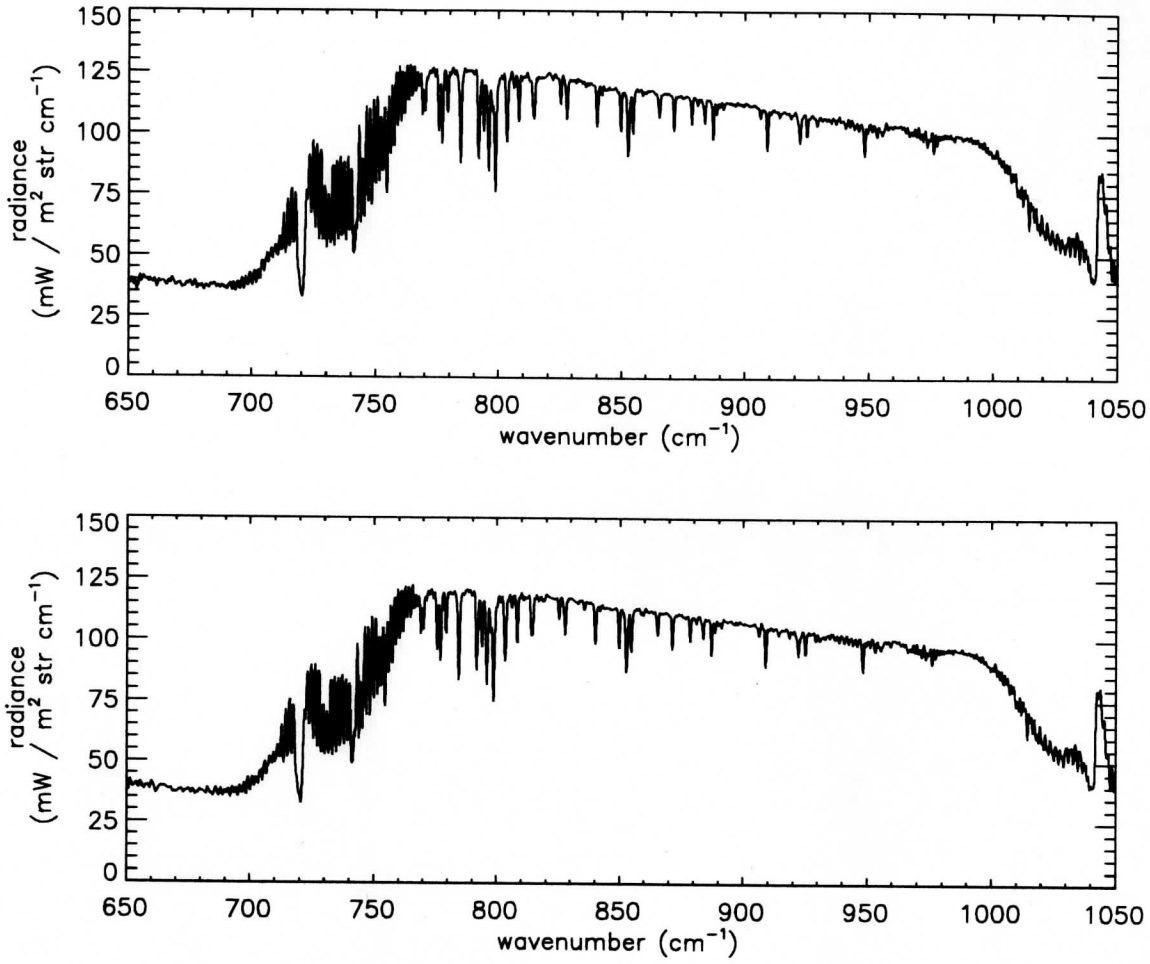

Figure 6. Two adjacent fields of view (2 km resolution) HIS radiance measurements viewing partial cloud and partial clear sky column radiance. The measurements are adjacent to each other with no more than one half of a field of view separation.

Computation of the N* cloud fraction ratio using the two measurements in figure 6 equals 0.268 which indicates a fair contrast exists between the two fields of view. High values of N* above 0.7 tend to be associated with adjoining fields of view with little scene contrast. High N*, small field of view contrast, are due to either extensive cloud contrast or relatively clear sky. This particular case is for two fields of view that

primarily view cirrus clouds as indicated in the MAS (1.85 μm) image in figure 7.

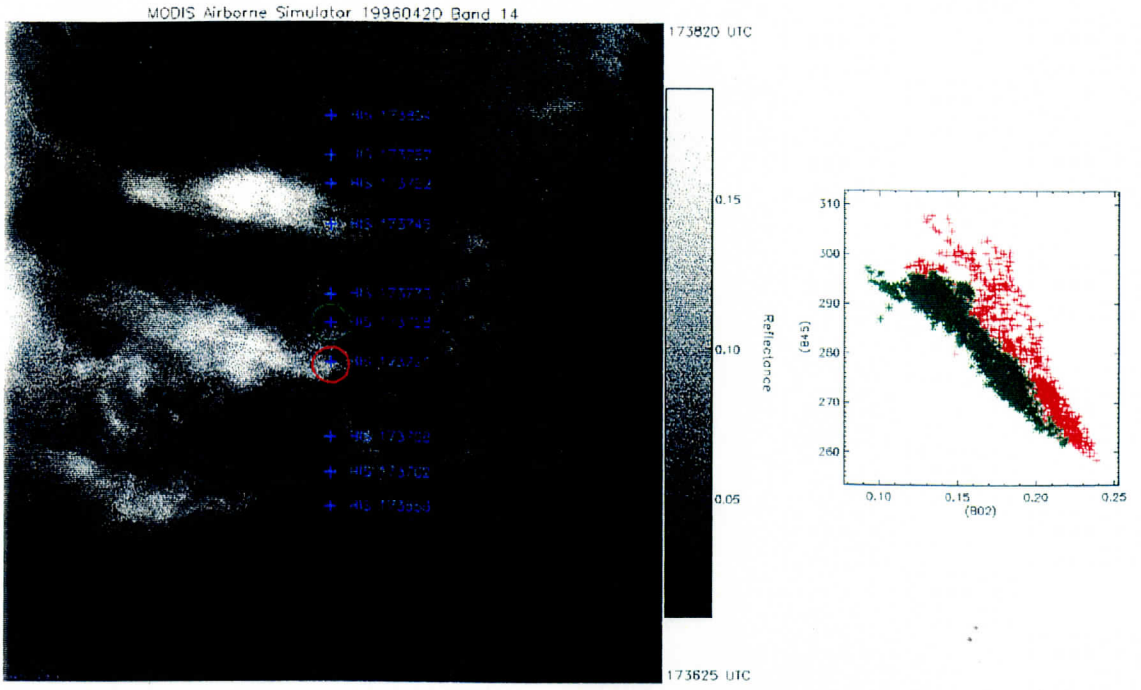

Figure 7. MAS (1.85 μm) image sensitive to cirrus clouds with HIS sampling times. The green and red circles denote the position of the HIS footprints used in the cloud clearing technique. The plot to the right of the image is a scatter plot of 11 μm brightness temperature versus 0.66 μm reflectance for the green and red circles.

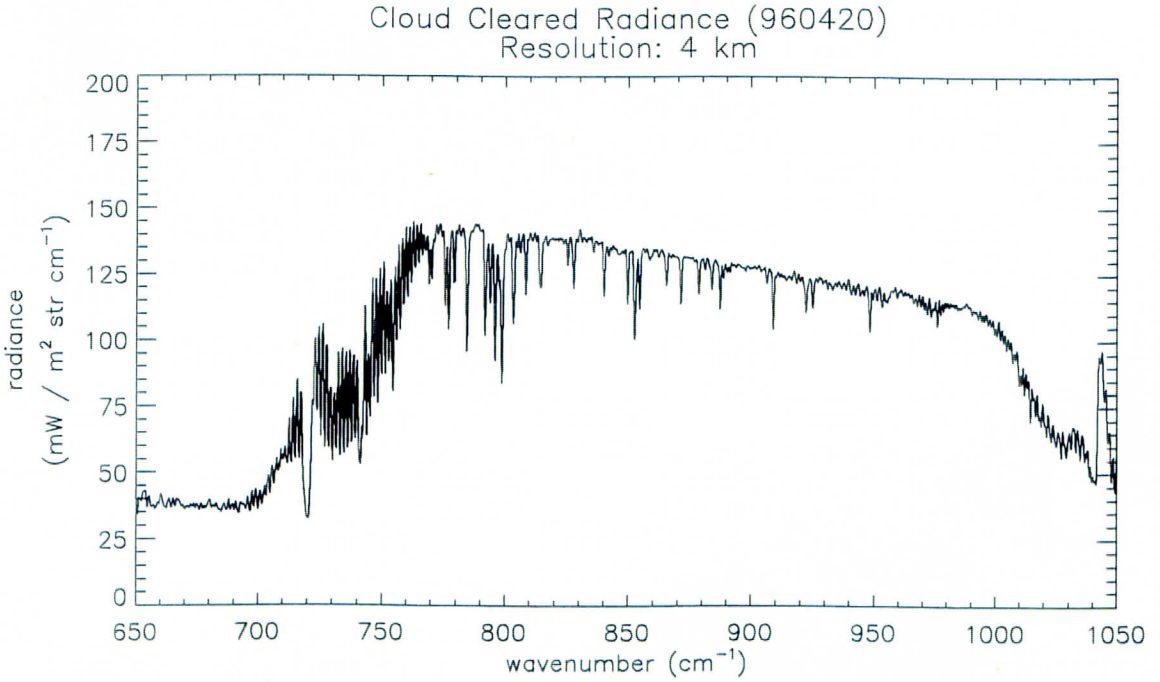

Figure 8. Cloud cleared radiance spectra obtained using the N* technique upon the radiance spectra depicted in figure 6. The field of resolution for this case is 4 km or two HIS fields of view.

The scatter plot of 11 μm brightness temperature versus 0.66 μm reflectance is consistent with the HIS measurements in figure 6. Application of the N* technique to this case resulted in a cloud cleared radiance spectra, figure 8, and it is equivalent to the HIS local clear radiance spectra in figure 5.

Figure 9 is a sample of the cloud clearing technique applied to two spatially averaged HIS radiance spectra used to simulate a field of view with a resolution of 4 km. The two radiance spectra in figure 9 are viewing single layer cirrus with the top layer at an altitude of 10,022 meters as indicated by the CLS data. The cloud fraction

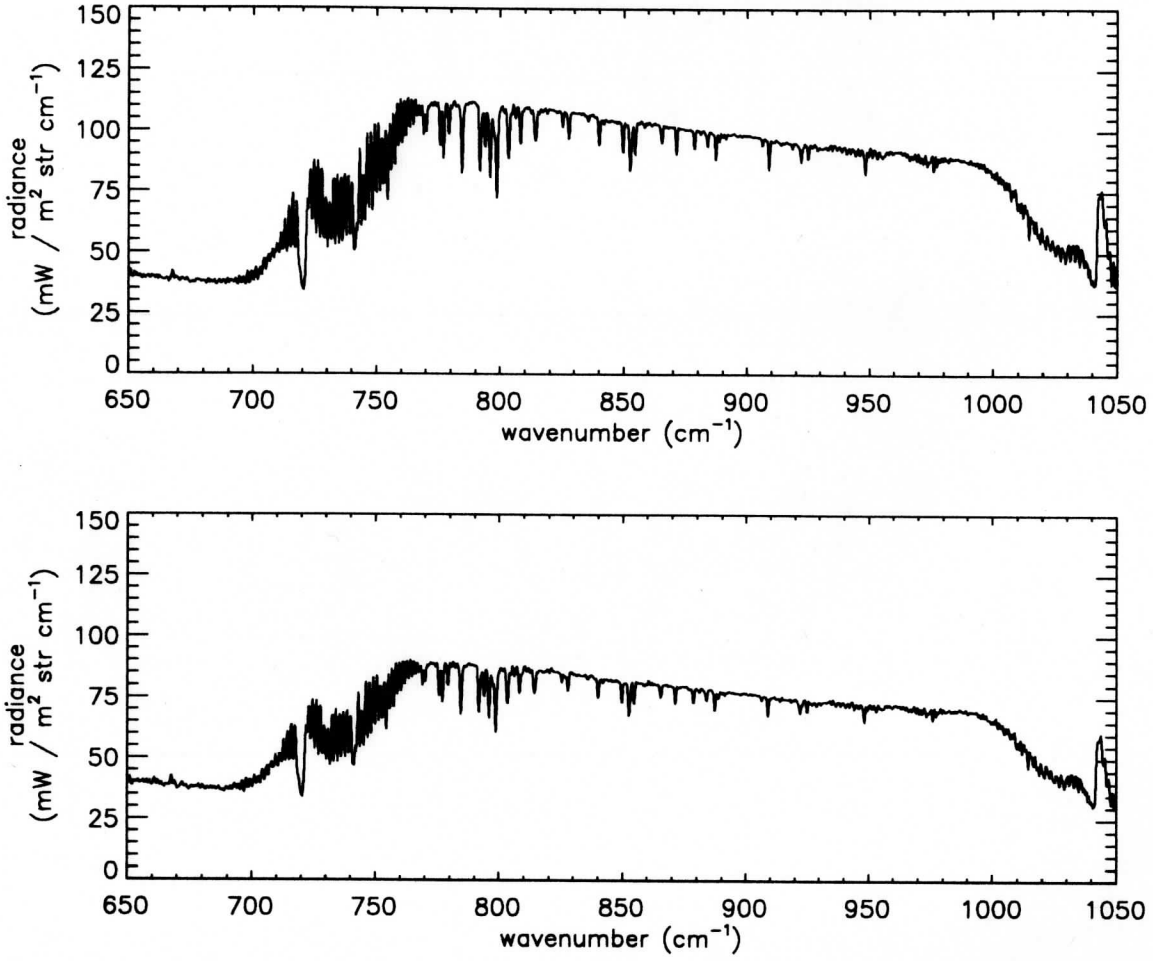

Figure 9. Each radiance spectra is an average of two HIS radiance measurements which simulate a 4 km field of view resolution. Both spectra show low radiance values indicative of clouds within the field of view.

amount ratio computed from the two radiance spectra depicted in figure 9 equaled 0.532 which indicates a moderate contrast exists between the two fields of view. MAS visible imagery of the area of interest shows each respective HIS footprint, figure 10, are predominantly obstructed by cirrus. The resultant cloud cleared product, figure 11,

yields a "declouded" radiance spectrum with an 8 km simulated resolution that is similar to the local 2 km clear sky HIS measurement - figure 12. Differences in the brightness

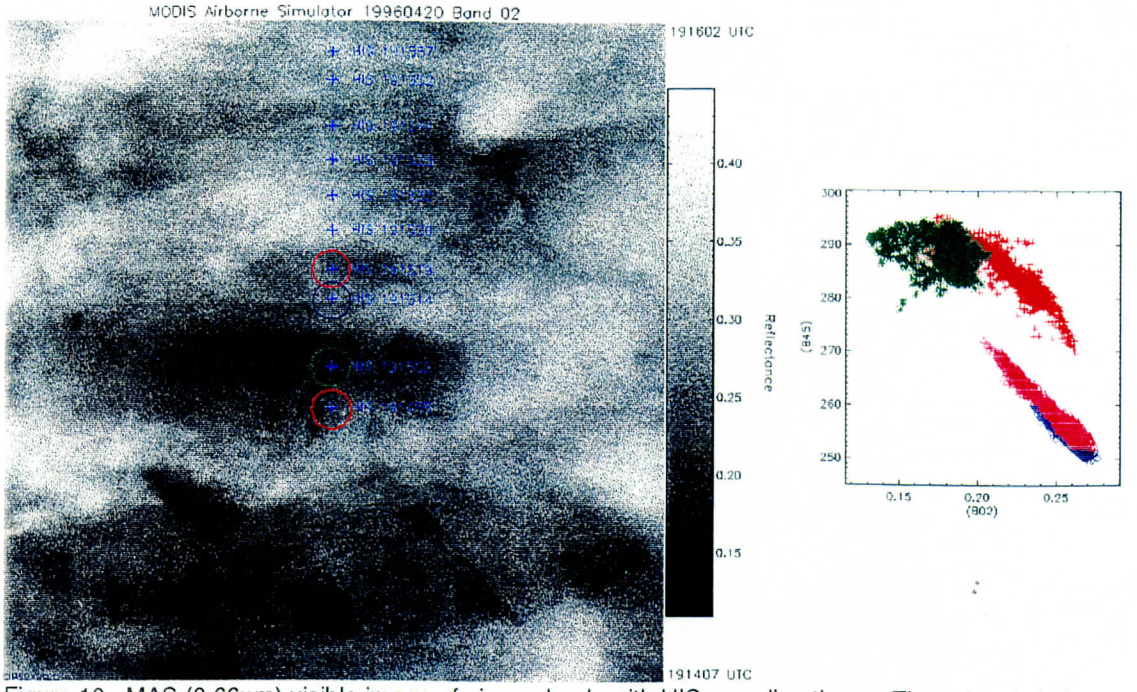

Figure 10. MAS (0.66μm) visible image of cirrus clouds with HIS sampling times. The colored circles denote the position of the HIS footprints used in the cloud clearing technique. The scatter plot to the right of the image is a scatter plot of 11 μm brightness temperature versus 0.66 μm reflectance for each respective colored circle.

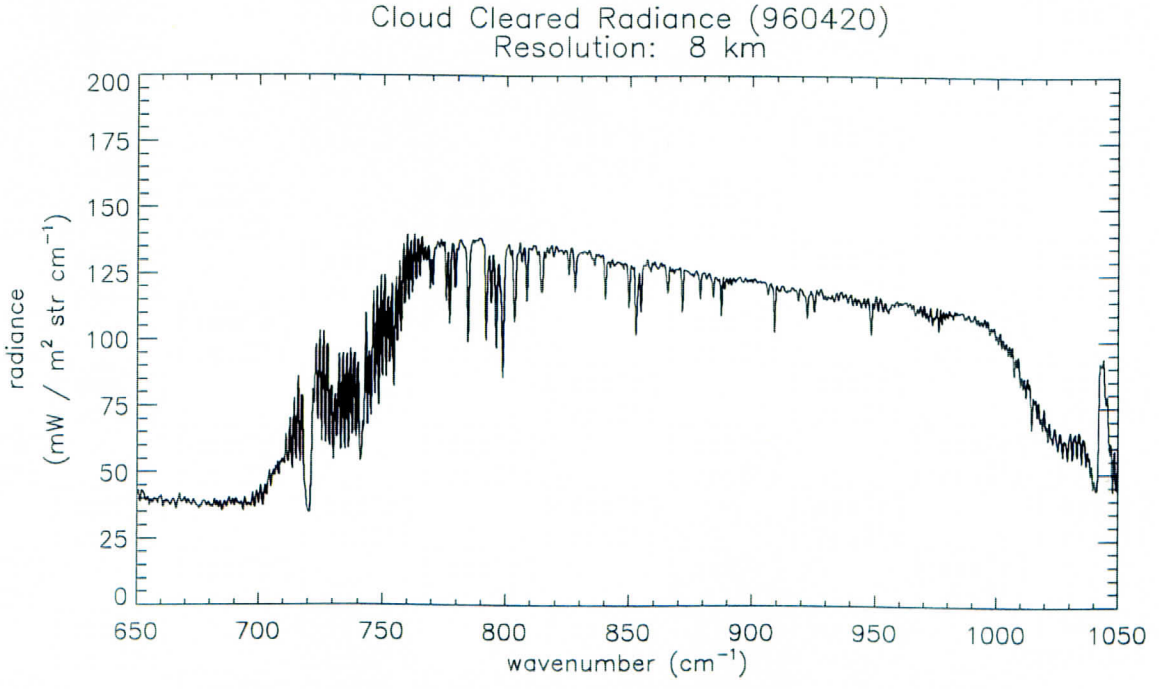

Figure 11. Cloud cleared radiance spectra obtained using the N* technique upon the radiance spectra depicted in figure 9. The field of resolution for this case is 8 km or two 4 km fields of view.

temperature between the local clear sky HIS measurements and the N* cloud cleared brightness temperature are generally within +/- 2 degrees Kelvin which is a favorable preliminary result - see figure 13.

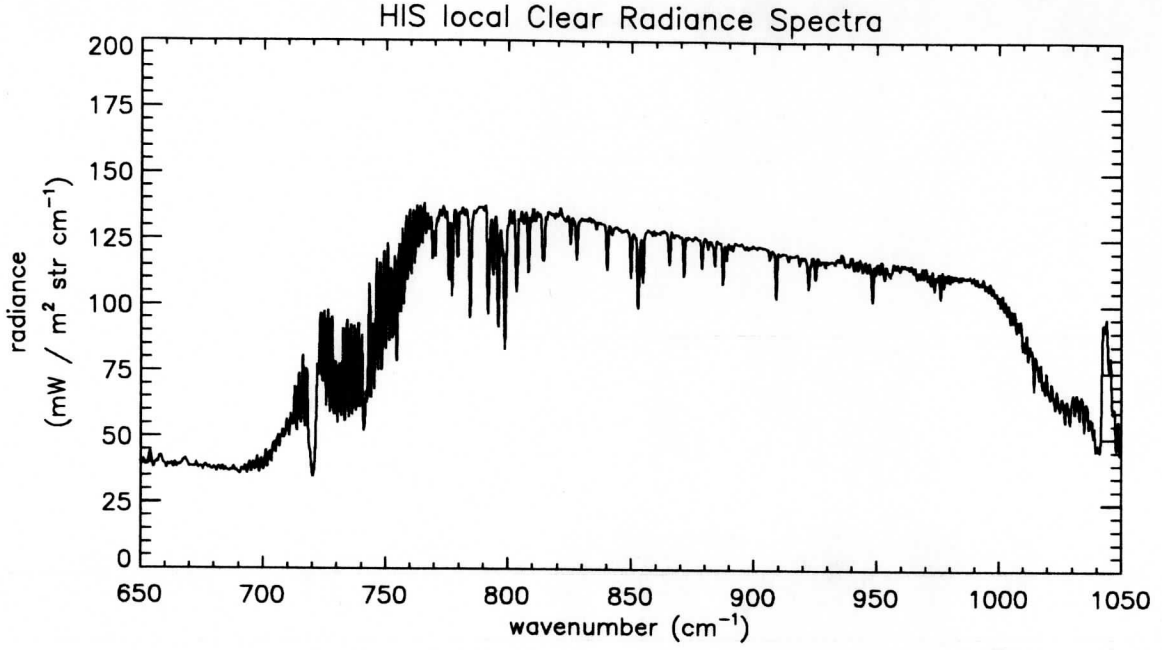

Figure 12. Local Clear sky HIS radiance measurement for wavenumbers 650 - 1050 cm^{-1} for SUCCESS case 960420. The spatial resolution of the field of view measurement is 2 km.

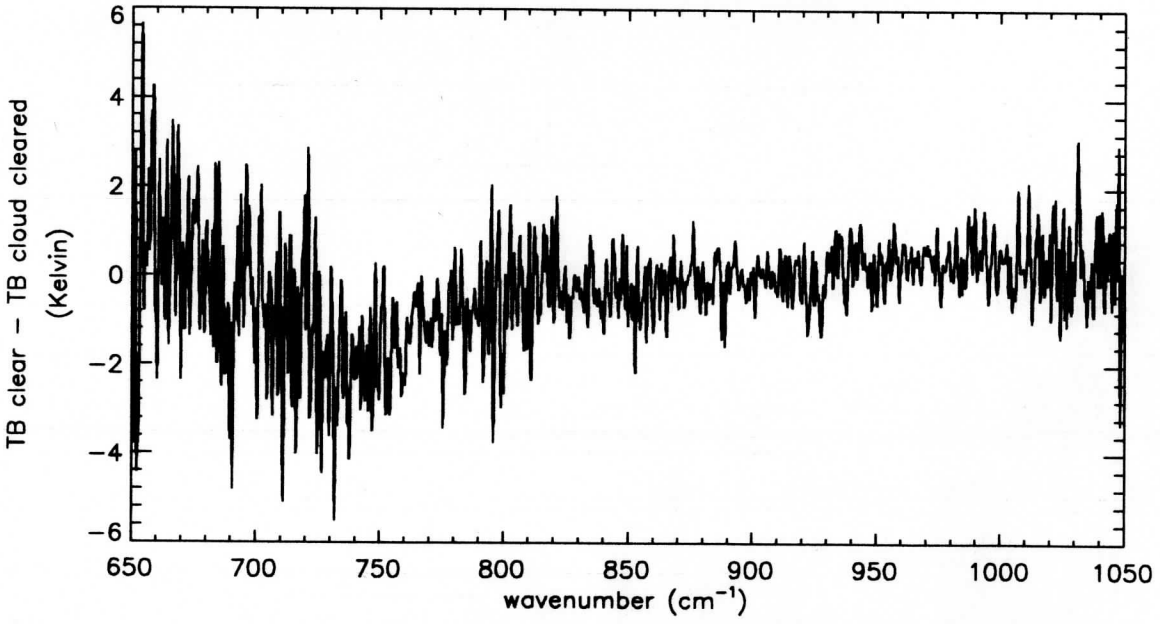

Figure 13. Brightness temperature differences between the local clear sky measurement and the cloud cleared technique by wavenumber.

Decreasing the resolution in the cloud clearing process to 16 km by using two fields of view yields two new footprints of four spatially averaged HIS field of view radiance measurements. Figure 14 depicts a sample of two such fields of view which are partially or fully obstructed by cirrus at an altitude of 10,062 meters. The cloud fraction ratio, N*, computed from the two spectra in figure 14 equaled 0.438 which is indicative of moderate cloud / clear sky contrast. Figure 15, the MAS 0.66 μm visible image

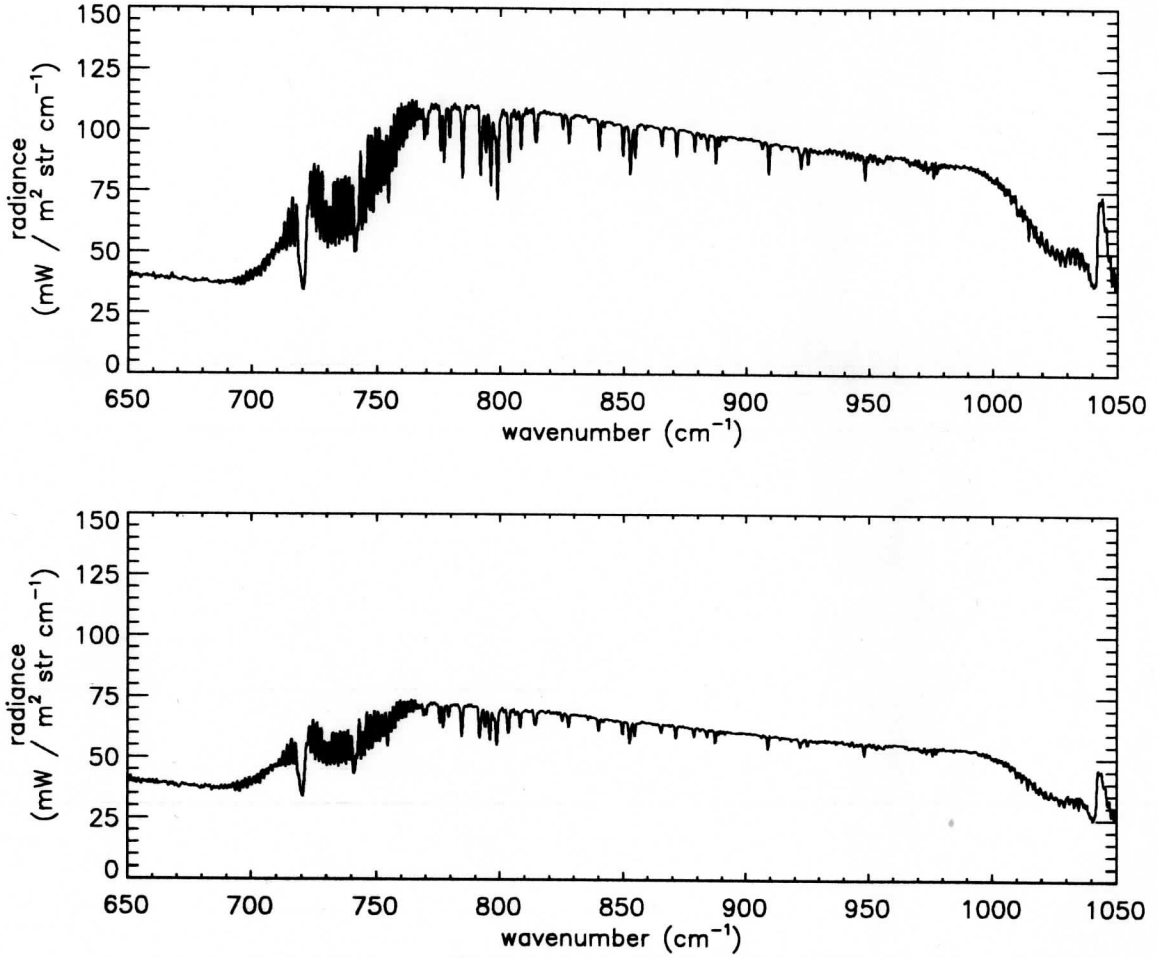

Figure 14. Each radiance spectra is an average of four HIS radiance measurements which simulate an 8 km field of view resolution. Both spectra show low radiance values indicative of clouds within the field of view.

which shows the location of the spatially averaged 8 km field of view, and the scatter plot of 11 μm brightness temperature versus 0.66 μm reflectance denote a significant difference between the two fields of view which are represented by the rectangles. The cloud clearing method applied to the 8 km fields of view in figure 14 produces a 16 km resolution spectrum, figure 16, that is similar to the local 2 km HIS clear sky radiance

spectra seen in figure 17. This cloud cleared spectrum is equivalent to the clear sky despite the decreased resolution of 16 km. The brightness temperature differences

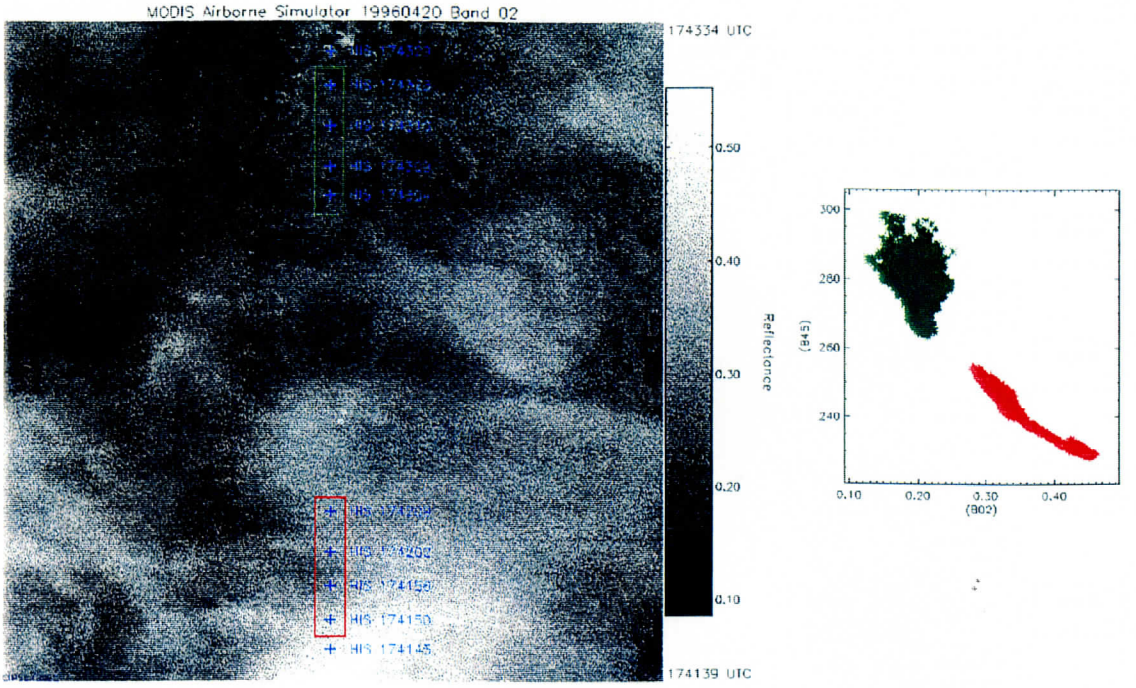

Figure 15. MAS (0.66μm) visible image of cirrus clouds with HIS sampling times. The colored rectangles denote the position of the HIS footprints used in the cloud clearing technique. The scatter plot to the right of the image is a scatter plot of 11 μm brightness temperature versus 0.66 μm reflectance.

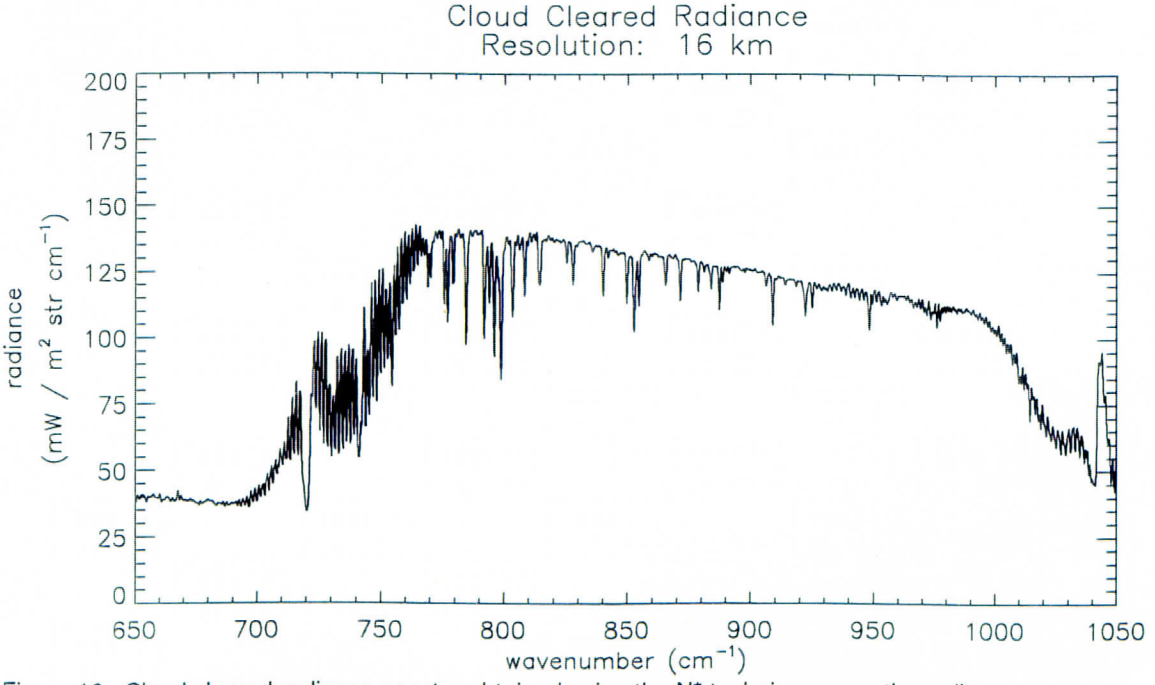

Figure 16. Cloud cleared radiance spectra obtained using the N* technique upon the radiance spectra depicted in figure 9. The field of resolution for this case is 16 km or two 8 km fields of view.

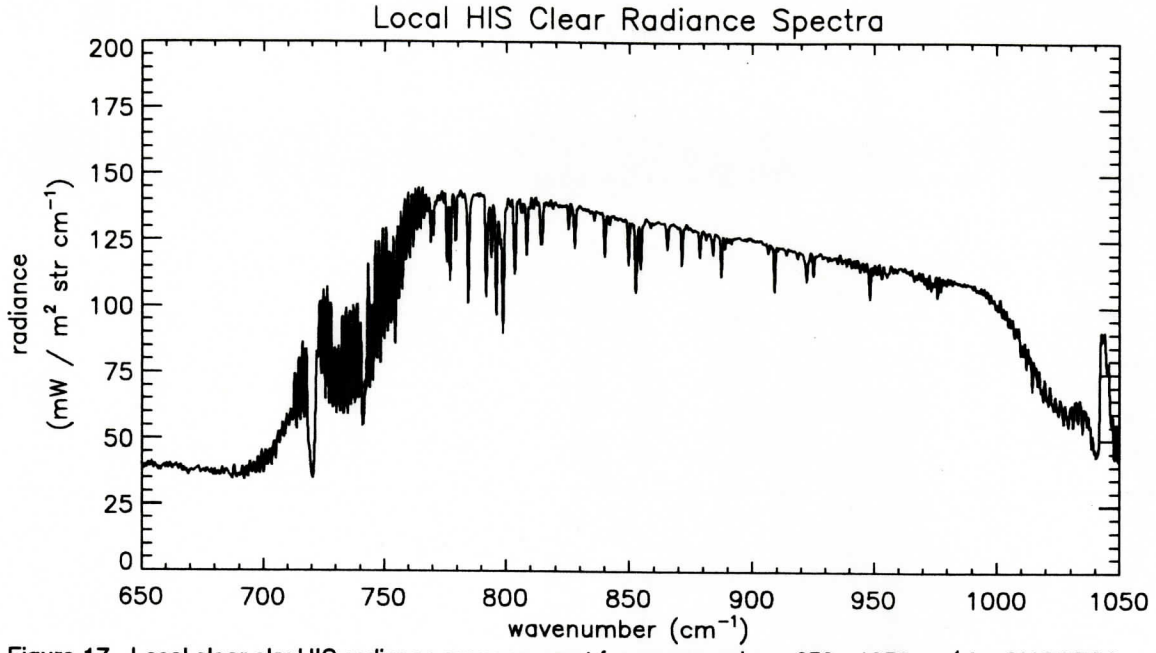

Figure 17. Local clear sky HIS radiance measurement for wavenumbers 650 - 1050 cm^{-1} for SUCCESS case 960420. The spatial resolution of the field of view measurement is 2 km.

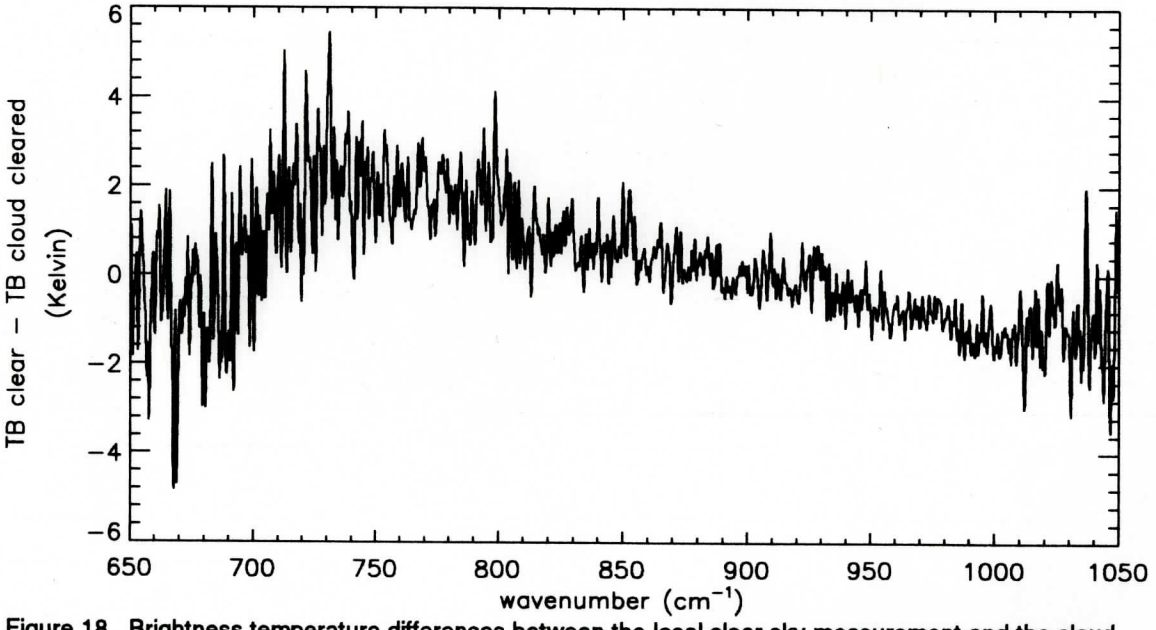

Figure 18. Brightness temperature differences between the local clear sky measurement and the cloud cleared technique by wavenumber.

between the clear sky and cloud cleared example, figure 18, are generally within +/- 2 degrees Kelvin in the window region with some variation by wavenumber between the clear sky and cloud cleared spectra. These variations are less pronounced in figure 13. Further study into decreasing the resolution and brightness temperature differences between clear sky and cloud cleared measurements will hopefully resolve whether

these variations are a function of the degradation in resolution or whether this is purely an isolated event.

The N* technique can be applied to include a larger wavenumber range. Figure 19 is a case depicting two adjacent HIS radiance measurements ranging from 600 to 2800 cm^{-1} with a 2 km field of view resolution. Clouds are present within each field of view as indicated by the low radiances. Application of the N* technique upon the

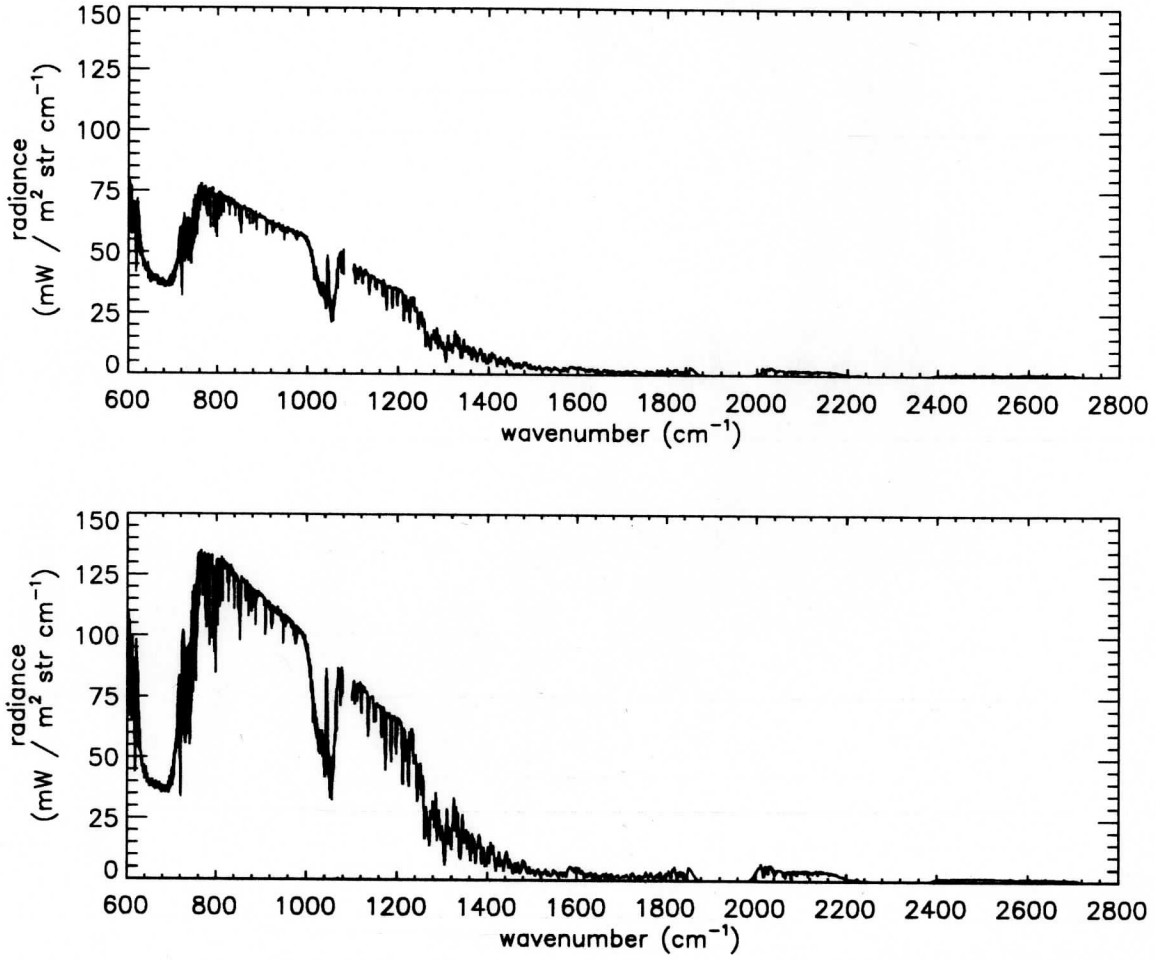

Figure 19. Two independent radiance measurements with full cloud cover within in the field of view (top) and partial cloud cover within the field of view (bottom). The resolution of these measurements is 2 km and wavenumber (wavelength) range from 600 cm^{-1} (16.7μm) to 2800 cm^{-1} (3.6 μm).

spectra in figure 19 produces a cloud cleared spectra comparable to the HIS local clear radiance measurement - figure 20. Since the cloud cleared radiance is similar to a locally clear air radiance spectra, validation can be accomplished in a two-fold manner. First, validation is done by comparison of the cloud cleared radiances against local

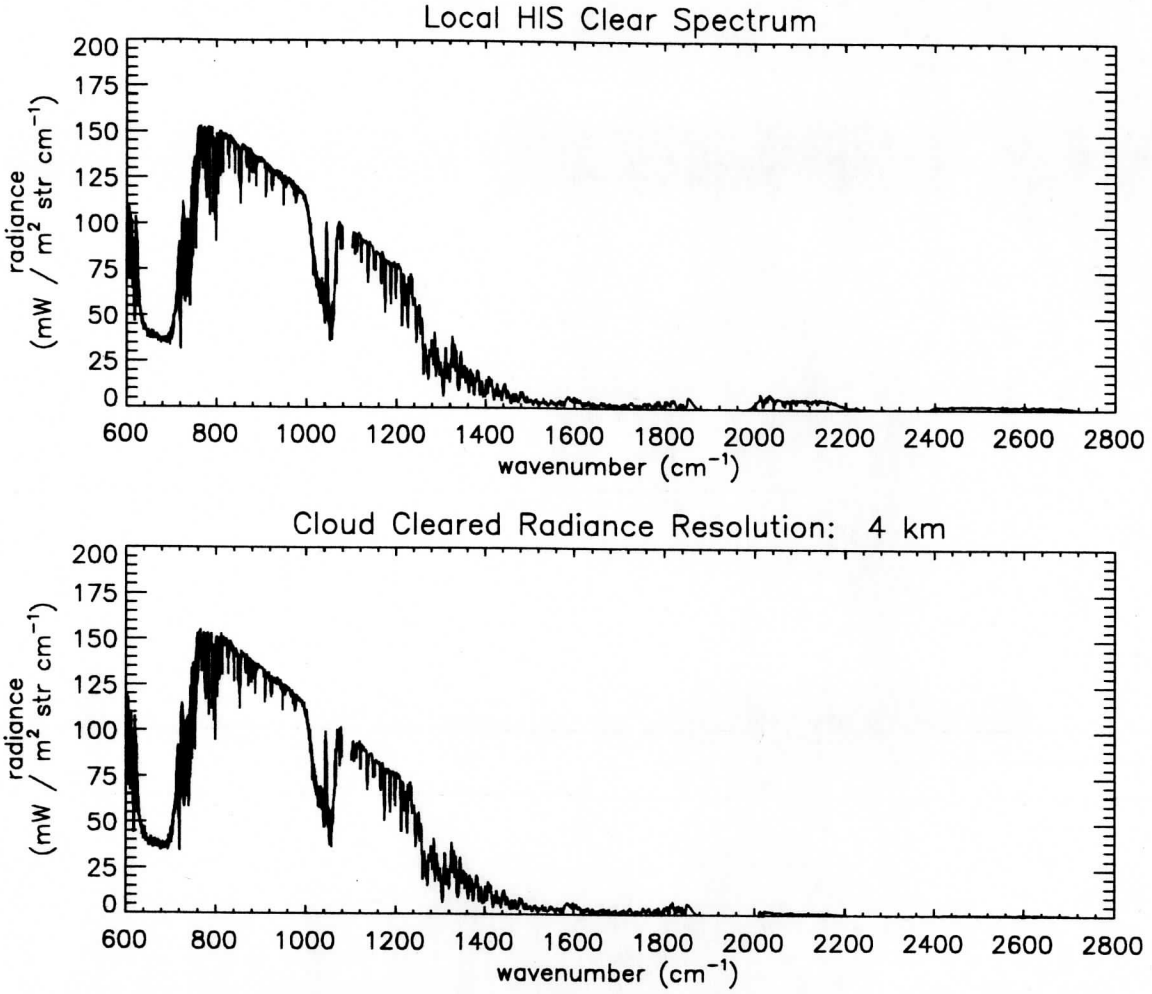

Figure 20. Local HIS clear radiance measurement and the cloud cleared radiance (top) measurement (bottom). The resolution of the top measurement is 2 km and the resolution of the cloud cleared radiance is 4 km; Wavenumber (wavelength) range is from 600 cm^{-1} (16.7 μm)to 2800 cm^{-1} (3.6 μm).

clear measurements and validation is done against MAS channel radiances that are determined to be clear within the obstructed HIS field of view. The cloud mask algorithm (Ackerman et al., 1996) allows for explicit determination of those MAS fields of view which are classified as confident clear or obstructed by clouds in terms of confidence levels - confident clear, probably clear, undecided or obstructed. From this spectrally determined information, the MAS clear channels within the HIS field of view can be compared against those obtained using the cloud clearing technique. This synergistic use of MAS and HIS allows for validation of the N* method within the same geographic location whereas comparison of a locally clear radiance measurement could possibly introduce errors into the validation that result from differing temperature or water vapor profile variations on smaller scales.

Figure 21 shows both HIS clouded radiance spectrums for two HIS fields of view and also shows the clear radiance spectrum derived from the N* cloud clearing technique. The cloud cleared radiance spectrum is vastly improved with respect to the two clouded HIS radiance measurements.

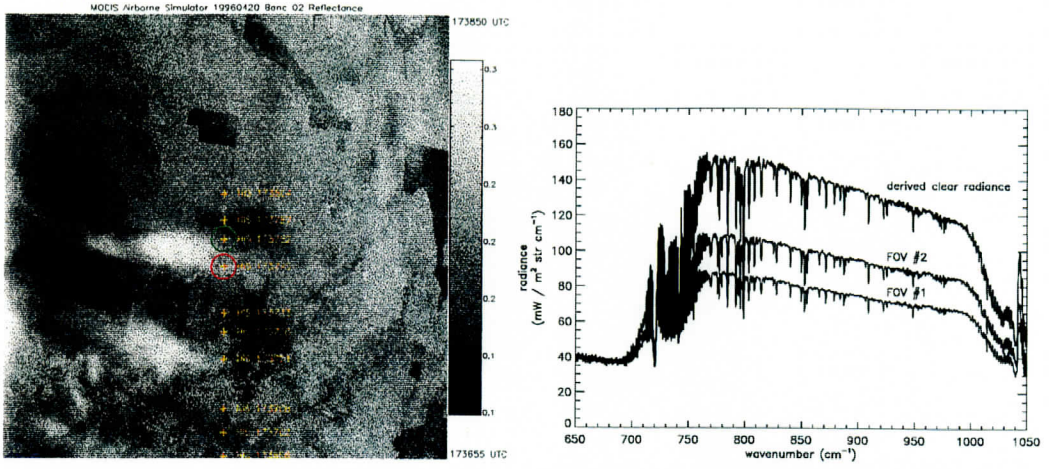

Figure 21. MAS visible (0.66 μm) image of cirrus clouds with HIS sampling times. The green and red circles denote the position of the HIS footprints used in the cloud clearing technique. The plot to the right of the image is the radiance spectrums of the two fields of view used in the cloud clearing process and the derived clear radiance spectrum.

Validation of the cloud clearing technique will provide additional confidence in the method and allow us to fully assess the RMS errors between clear and cloud cleared as a function of N* and the field of view resolution. The validation process will help to ensure a high confidence in the technique and help provide the necessary data required to make an informed judgment into which trade-offs between instrument field of view and signal-to-noise are necessary to yield the optimal instrument configuration needed to effectively obtain cloud cleared radiance measurements needed for accurate retrievals of temperature and water vapor. Figure 22 is an example on how validation of the cloud clearing technique will be done using a MAS and HIS synergistic approach. The cloud mask algorithm will be used to determine which portion of the interferometer field of view is clear and then spatial averaging of the cloud mask discriminated clear MAS radiances of each appropriate channel will be completed and summarily compared against the HIS cloud cleared radiances. The MAS cloud mask algorithm uses five spectral test categories to discriminate between clear and cloudy skies. These five tests, described further in Ackerman et al. (1996), are comprised of the following test groups: simple infrared threshold tests, brightness temperature difference

tests, solar reflectance tests, near-infrared tests for cirrus / thin cirrus, and infrared tests for cirrus / thin cirrus.

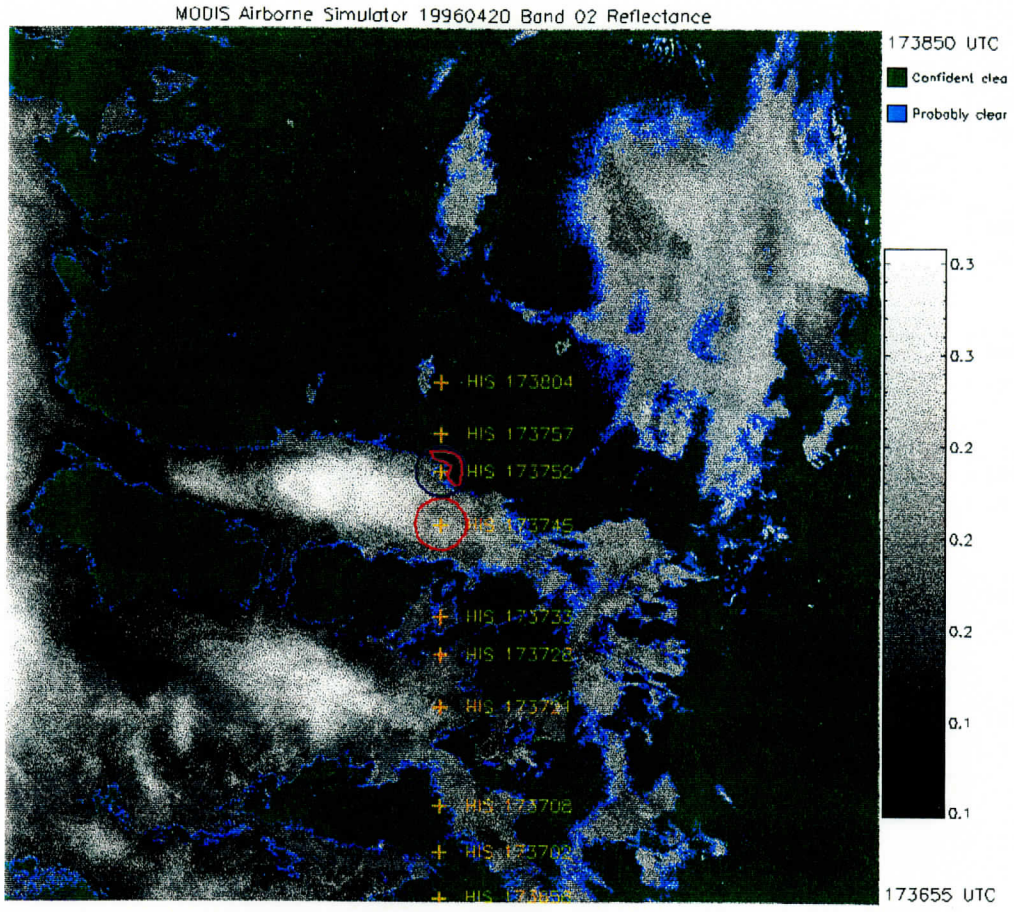

Figure 22. MAS visible (0.66 μm) image of cirrus clouds with HIS sampling times and cloud mask algorithm results depicting those areas that are determined as confident clear and probably clear. The blue and red circles denote the position of the HIS footprints used in the cloud clearing technique and the pink is the MAS cloud mask algorithm determined clear area within the HIS fields of view.

High clear confidences within the partially clouded fields of view used in the cloud clearing process will provide an opportunity to average the MAS high spatial resolution radiance measurements and compare them against the cloud cleared radiances. Figure 23 is a scatter plot of MAS clear air and local HIS clear field of view brightness temperatures, resolved using MAS spectral response functions, against the HIS cloud cleared brightness temperatures. The local HIS clear field of view brightness temperatures show good agreement with the brightness temperatures obtained from the cloud cleared radiances. The cloud mask determined clear area brightness temperatures within the partially clouded interferometer field of view are in reasonable agreement with the cloud cleared radiances. The existing differences are attributable to cloud shadows over the clear areas, figure 21, that are within the interferometer's

fields of view. The best agreement is for channel 42 (8.5 μm) through channel 46 (12.0 μm) in which the brightness temperatures are generally within 4 degrees Kelvin, whereas the other channels depart by no more than 10 degrees Kelvin. Clear areas outside of the interferometer field of view near the cloud edge and away from the shadow region reveal that the brightness temperatures for channels 42 through 50 are all within 2 degrees Kelvin for this particular case.

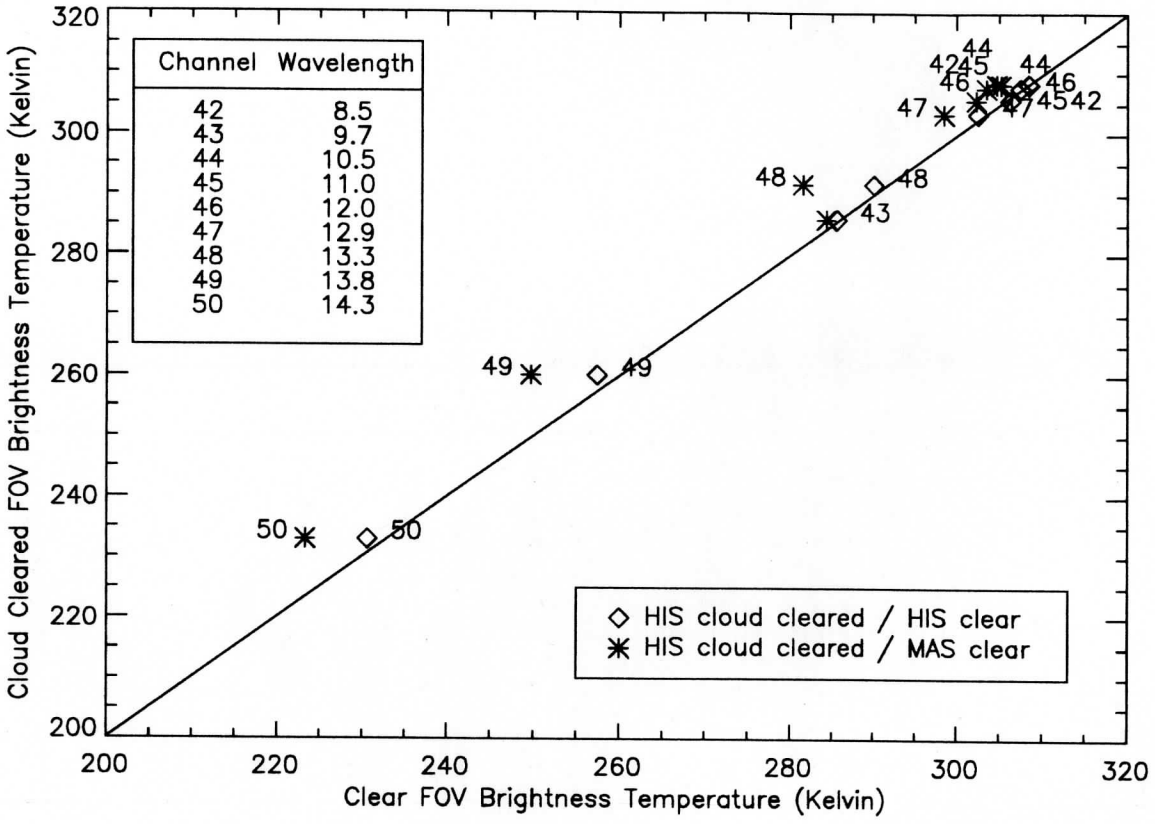

Figure 23. Scatter plot of the HIS cloud cleared against the MAS clear area within those HIS fields of view used in the cloud clearing process and against a HIS local clear field of view. Cloud cleared resolution is 4 km, HIS local clear resolution is 2 km, and MAS resolution is 50 meters times the clear area within those footprints used in the cloud clearing process.

Future work on this cloud clearing task using the available data sets from SUCCESS and WINCE will focus on producing statistics on the accuracy of the cloud cleared approach against the local clear area as a function of N* and instrument field of view. These data sets will then be implemented in the retrieval performance analysis to further differentiate between the field of view resolution and signal-to-noise as it pertains to making use of partially clouded radiance measurements by deriving clear

radiances from different resolutions. Retrieval software developed at CIMSS will be used to compute temperature and water vapor soundings using a non-linear physical retrieval algorithm and used in the validation process along with providing error statistics in terms of temperature and water vapor retrieval RMS error as a function of N* and instrument field of view resolution. Further comparisons may be added in the year two study to help clarify resolution and signal-to-noise issues as it relates to radiometric sounding in broken to overcast areas.

3.3 Clear and cloudy retrieval performance analysis

The three different retrieval methods, clear hole hunting, cloud clearing (N*) and direct simultaneous retrievals from clouded observations, will be applied to ITS, AMSU and MHS data using airborne simulated HIS and NAST data which was described previously in section 3.2. This analysis will use those data sets in the retrieval process to break down the results based on different sized field of view resolutions in order to specify the optimal CrIS spatial resolution requirements needed to ascertain an optimal trade-off that will offer the best sampling strategies and instrument configuration for the future NPOESS sounder. This task will be accomplished in year two of this study since tasks 1 and 2 will provide the required performance analysis data sets which are still in progress. Task 3 will determine the optimized trade-off necessary to satisfy both the technology constraints and scientific / operational goals necessary to successfully utilize the future Interferometer Thermal Sounder from a space based platform

3.4 Studies using IMG interferometer data from the Advanced Earth Observing Satellite (ADEOS)

The IMG (Interferometric Monitoring of Greenhouse Gases) instrument on the Japanese ADvanced Earth Observing Satellite (ADEOS) has made global observations of the infrared spectral radiance of the earth / atmosphere at very high spectral resolution. This particular task will validate retrievals from IMG data against selected ground truth sites, and well calibrated IMG data is necessary in order to correctly accomplish this task. Current analysis of IMG calibration issues and data quality assurance is being carried out by Dr. Hank Revercomb and Dr. Von Walden with support coming primarily from Space Science and Engineering Center internal funds. The data necessary to complete this assigned task hinges largely upon the work completed to date and future work yet to be accomplished by Dr. Revercomb and Dr. Walden in order to provide well calibrated datasets needed to perform robust retrieval

studies using IMG data which is well warranted for defining ITS requirements. Fiscal constraints may jeopardize issuance of this data or compromise the integrity of the datasets; therefore, it is advisable that outside funding be procured in order to ensure this particular task is completed with a high degree of confidence. Compliance of this task is set to commence in year two of this study; however, there is no assurance of completion of the calibration of the IMG data due to possible future internal budget constraints which may either hamper or eliminate the calibration project altogether. The proper calibration and analysis work must be continued; otherwise, results from an IMG retrieval study may not supply the necessary information required for this study.

The radiance observations from IMG can provide additional information needed to define which resolutions and spectral coverage requirements are needed for an earth observing interferometer from space. IMG's broad spectral coverage (3.3 μm - 14 μm) does provide sufficient sampling of all the main temperature and water vapor sounding regions at a high apodized spectral resolution of 0.1 cm^{-1} and with a spatial resolution of 8 km. Still, only one complete spectral observation is made every 86 km along the satellite's nadir track, but past data will nonetheless provide additional information on the performance of an interferometer from space that should benefit in how best to satisfy the operational and scientific goals of an ITS under the weight and power constraints imposed by the NPOESS system.

This task will involve collection of past IMG data and co-locating those specific observations with ground truth sites in order to evaluate retrieval accuracy as a function of spectral resolution and instrument response function shape. Furthermore, the IMG's high resolving power allows one to accurately simulate observations of lower resolution instruments such as the ITS. The lower resolution IMG simulated retrievals will then be compared against the full resolution IMG retrievals to evaluate the differences between using higher resolution versus lower resolution. Figure 24 is such an example of the IMG's full resolution along with simulating a lower resolution interferometer such as NAST. Comparisons of the two differing resolutions using space borne interferometric data will help substantiate if any large discrepancies exist between higher resolution or lower resolution interferometer radiance observations.

The collection of IMG data will take advantage of retrieval studies made during the field campaign "WINCE" where several ground truth sites are available. Figure 25 shows a GOES visible image for 28 January 1997 with the flight track of the ER-2 which

shows a GOES visible image for 28 January 1997 with the flight track of the ER-2 which carried both the HIS and MAS instruments. Also depicted are the IMG spectral observations taken every 86 km and the associated ground truth sites which will provide valuable data to improve upon sounding retrieval algorithms from a space based sun-synchronous system. Figure 26 shows the resultant IMG radiance spectra taken at location IMG 6 which is co-located along the ER-2 flight path.

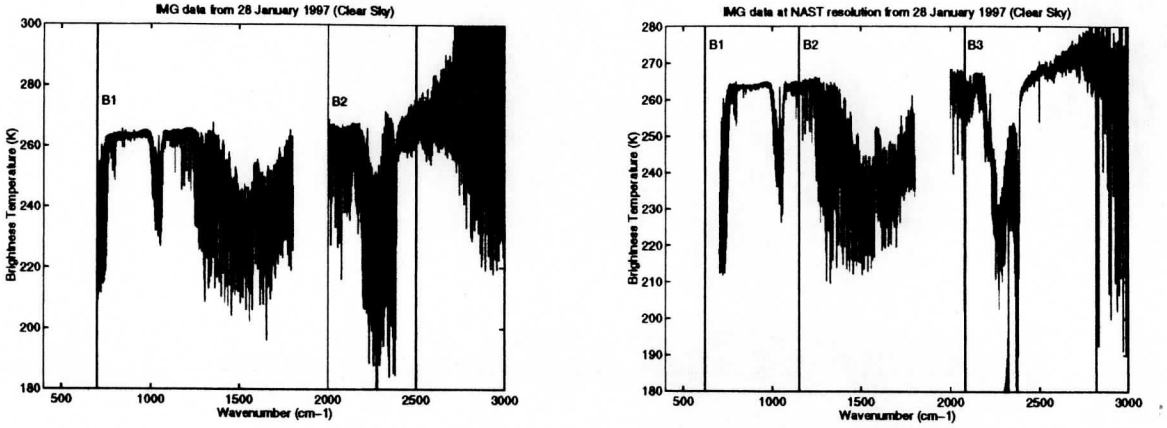

Figure 24. Plot A is the clear sky brightness temperatures computed from clear sky radiance observations taken at the full IMG spectral resolution. Plot B is IMG data used to simulate lower resolution NAST data for the same clear sky radiance observations. (provided by Dr. Revercomb and Dr Walden, Space Science and Engineering Center)

The original IMG spectra and corrected spectra are depicted in figure 26 along with the difference between the two radiance spectra - the differences are significant between the original and corrected spectra - 10% differences occur for this case. Quality assurance of data and data processing is of the utmost importance since the discrepancies shown in figure 26 can lead to erroneous conclusions once the retrieval simulation study is completed. However, the IMG data with the corrected data will be quite useful for this particular study. Figure 27 which is a plot of the HIS and IMG radiance observations in the CO_2 region are quite similar. The IMG resolution has been reduced to HIS resolution, and the HIS and IMG spectra are offset by +40 in order to easily see the marked similarity between the HIS spectra and the IMG reduced to HIS resolution spectra. Using the IMG data to simulate various resolutions is certainly representative of lower resolution data as shown in figure 27, and will provide a useful assessment of retrievals between IMG full resolution and the lower spectral resolution proposed for the ITS instrument.

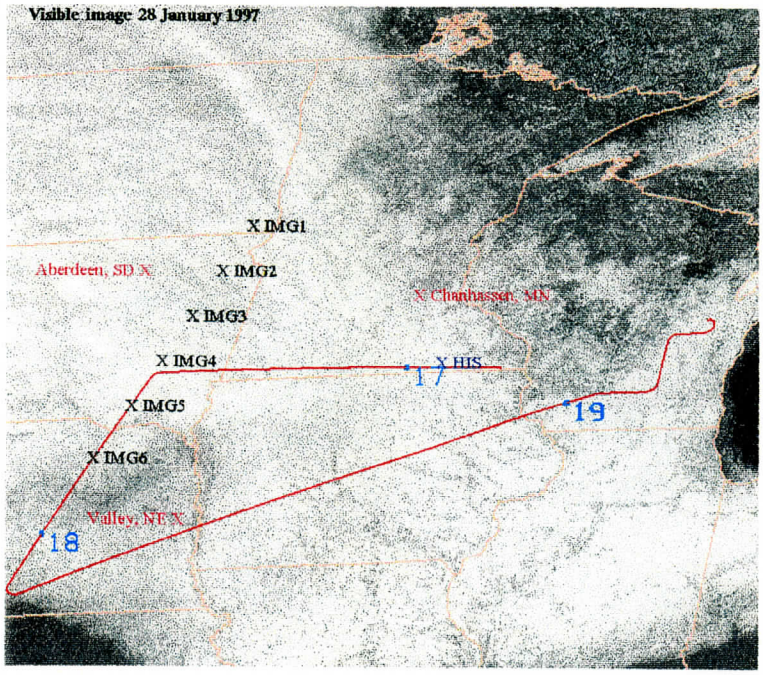

Figure 25. GOES visible image for 28 January 1997 during the WINCE field campaign. ER-2 flight track and ADEOS IMG spectral observations are overlaid upon the visible image. Also depicted are three viable ground truth sites which could be used in a performance analysis.

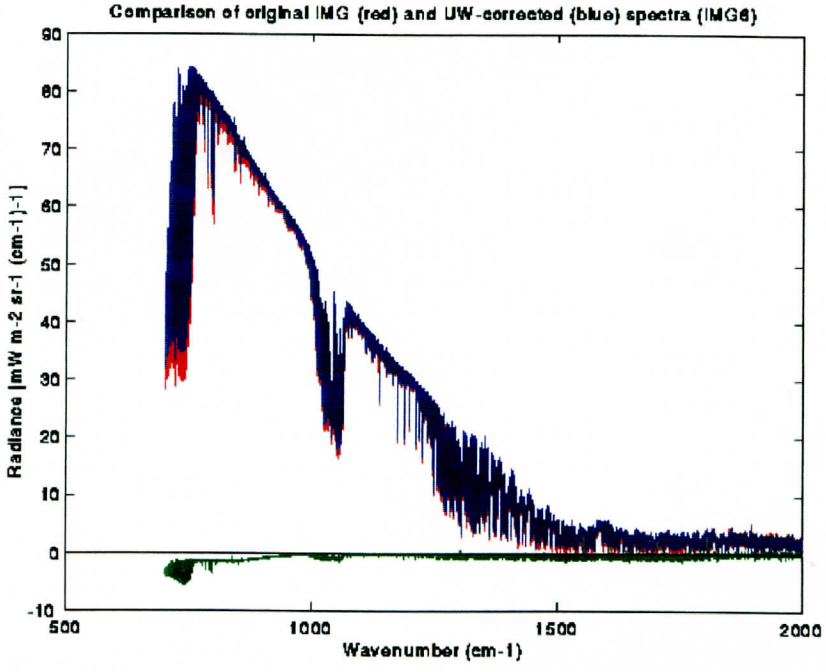

Figure 26. The original IMG and corrected radiance spectra for location IMG 6 depicted on the GOES visible image in figure 25. Residual between the original and corrected radiance spectra is depicted in green (provided by Dr. Revercomb and Dr. Walden, Space Science and Engineering Center).

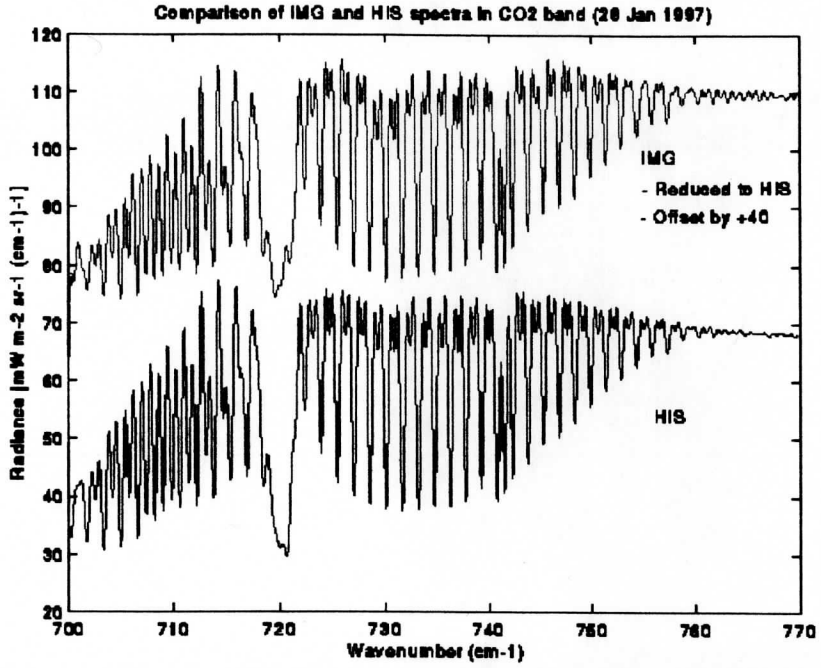

Figure 27. Comparison of IMG and HIS co-located spectra in the CO_2 band. IMG spectra is reduced to HIS resolution and an offset of +40 is introduced to show CO_2 absorption lines. (provided by Dr. Revercomb and Dr. Walden, Space Science and Engineering Center)

3.5 NAST scientific algorithm development

The NPOESS Atmospheric Sounding Testbed - Interferometer (NAST-I) (Cousins and Smith, 1997) is being developed to make infrared spectral radiance measurements for the National Polar-Orbiting Operational Environmental Satellite System. The interferometer is designed to fly on the ER-2 with a nominal spatial resolution of 3 km within a swath width of about 50 km from the flight altitude of 65,000 feet (20 km). The NAST-I is a heritage of the non-scanning HIS with a spectral coverage of 3.6 - 16.1 μm and an unapodized spectral resolution of ≈0.25 cm^{-1} which makes this NAST-I capable of simulating any of the future infrared sounding instruments proposed for the NPOESS.

NAST-I, to be deployed during CAMEX-III, will fly in the right superpod of the NASA ER-2 making spectral measurements for use in deriving NPOESS EDR's physical variables, such as atmospheric temperature and water vapor profiles, land and sea surface temperature and emissivity, and cloud geometric and optical properties. The NAST data processing and retrieval algorithm are designed to take advantage of the data analysis experiences learned from using HIS aircraft measurements and AIRS

simulations. There are two types of retrieval strategies that are employed based on the following set of criteria: 1) when only infrared data are available, and 2) when both infrared and microwave data are available.

The radiative transfer equation written in perturbation form (linearized from a first guess initial state) becomes

$$\delta T_B = T_B - T_B^0 = W_{T_s} \delta T_S \int_0^P W_T \delta T(P) dP + \int_0^P W_Q \delta Q(P) dP \quad (1)$$

where δ denotes a departure from the initial state, T_B is the NAST brightness temperature, and the superscript denotes the initial state. T_s, T(P), and Q(P) are unknowns of surface skin temperature, temperature, and water vapor mixing ratio profiles. W_{T_s} and W_T, and W_Q are Jacobian matrices of surface skin temperature, temperature, and water vapor, respectively.

A hybrid non-linear Newtonian iteration scheme which incorporates the inverse Hessian and steepest descent methods is used to solve (1). This iteration scheme is adapted from the early work of Levenberg and Marquardt. The Levenberg-Marquardt (L-M) method is formulated as

$$Y_{n+1} = Y_n - \left[\nabla^2 \chi_n^2 + \gamma I\right]^{-1} \nabla \chi_n^2 \quad (2)$$

where Y is the vector of retrieval variables (T_s, T(P), and Q(P)). Y_n and Y_{n+1} are the previous and current solutions, respectively. γ is a conditioning parameter used to control the rate of convergence. If γ is very small, this method tends to the inverse Hessian method; if γ is large, it tends to the method of steepest descent with a small solution size. For each iteration, a value of γ is chosen so that the method of steepest descent is used when far from the solution, and the inverse Hessian method is used when near the solution. This is accomplished by using the following criterion:

If χ^2 **increases** (solution divergence), **increase** γ and do **not** update Y_n

If χ^2 **decreases** (solution convergence), **increase** γ and **update** Y_n

χ^2 is defined as,

$$\chi^2 = (T_B - F(Y_n))^T \left(W_n S^{-1} W_n^T + S_b^{-1}\right)^{-1} (T_B - F(Y_n)) \quad (3)$$

where F is the forward model, and W is the Jacobian of the temperature and water vapor profile and surface skin temperature. S is a diagonal matrix representing the covariance of the NAST data noise. S_B^{-1} is the first-guess error covariance and usually

is assumed to be ignored when it is not well known. Rewriting (1) into iterative form given by (2), we obtain

$$Y_{n+1} = Y_0 + \left(W_n^T S^{-1} W_n + S_b^{-1} + \gamma I\right)^{-1} \left(W_n^T S^{-1}\left([T_B - F(Y_n)] + W_n(Y_n - Y_0)\right) + \gamma(Y_n - Y_0)\right) \quad (4)$$

Equation (4) then forms the basis of the NAST retrieval system prior to eigenvector transformations. Again, Y_0 denotes the initial first guess state of retrieval variables.

Eigen-transformation of (4) is performed to take advantage of the reduction of variables of Y which produces a stable inverse retrieval solution.

$$Y_{n+1} = Y_0 + \phi\left(\phi^T W_n^T S^{-1} W_n \phi + \gamma\lambda^{-1}\right)^{-1} \left(\phi^T W_n^T S^{-1}\left([T_B - F(Y_n)] + W_n\phi(Y_n - Y_0)\right) + \gamma(Y_n - Y_0)\right) \quad (5)$$

where ϕ consists of the first 15 temperature profile eigenvectors (corresponding to the largest 15 temperature eigenvalues) and the first 10 water vapor eigenvectors (corresponding to the largest 10 water vapor eigenvalues). The choices of these numbers are based on the information content analysis of HIS and other high spectral resolution infrared sounders (CIMSS report, 1997). λ is a diagonal matrix consisting of associated eigenvalues of these eigenvectors and some ad-hoc value for the conditions of the surface skin variable. The dimensions of the matrix

$$\left(\phi^T W_n^T S^{-1} W_n \phi + \gamma\lambda^{-1}\right) \quad (6)$$

to be inverted has been reduced from 85 x 85 in (4) to 26 x 26 in (5) for the clear retrieval conditions. This reduction in dimensionality reduces processing time and improves the stability of the retrieval solution. The same retrieval principle has been applied to HIS field experimental data.

When microwave data are available, the microwave T_B is also used in the solution (5) where microwaves penetrating through clouds can help to yield a reliable non-precipitating cloudy retrieval. Usually, the surface emissivity of microwaves (which, unlike infrared, is far from unity and needs to be dealt with due to significant components from surface reflection) is an additional unknown to be solved simultaneously or accurately predetermined prior to this inverse process. When microwave data are not available, the algorithm is modified to include the cloud effects in the measured radiances by assuming that below the cloud level the retrieval temperature is the same as cloud temperature (i.e., isothermal below cloud level). The temperature regression first guess profiles are processed in this way to reflect an isothermal effect below cloud level when cloudy profiles are detected.

4.0 Future Work

Funding for continued study of the five tasks described in section 3 has been selectively scaled down for the next year in this effort, and in response we have been forced to amend our initial task load to number three tasks. These three tasks represent a limited study which is hoped to provide the best possible study into assessing the instrument trade-offs needed to meet NPOESS engineering constraints for instruments to meet operational and scientific goals.

4.1 Future Work: Development of a sampling strategy for optimizing retrievals under partly cloudy conditions

During the early portion of year two of this study, the MAS data and applied cloud mask algorithm which discriminates between clear and cloudy skies will be implemented to study the probability of obtaining a clear field of view for several field of view resolutions. The use of the cloud mask algorithm determined clear / cloud probabilities will focus on several different sampling strategies and field of view resolutions using calibrated level 1B data sets from the following field campaigns: ARMCAS (April 1995), SCAR-B (August - September 1995), SUCCESS (April - May 1996), and WINCE (January - February 1997) with the possibility of adding other field campaigns as these data sets become available. MAS images will be used to determine those areas which are comprised of broken to overcast cloud cover for use in the analysis. These clear / cloud probabilities will also be used to study the effect of increased detector noise in clear air radiance data as a function of increasing the field of view resolution.

Further simulations using real data will study the effect of increased detector noise upon the retrieval accuracy of clear air radiance data and different field of view resolutions will be accomplished in year two. CLS cloud height information, MAS 50 meter imagery, and MAS cloud mask algorithm results will be used in combination to define which HIS fields of view are unobstructed by cloud cover. These HIS cloud free spectra will then be spatially averaged to simulate different field of view resolutions within a 90 km track. Retrievals done using this data will then be performed using a non-linear physical retrieval algorithm which produces temperature and water vapor profiles. These profiles will be used as the clear air "truth" for which all comparisons will be made against. Artificial detector noise will then be added to the clear air spectrum as described in section 3.1 to simulate noise effects that would be encountered by increasing the field of view resolution. The retrieval process will be performed on these

results and compared against the clear "truth." Differences in the noise induced retrievals and the "true" retrievals will support which field of view resolutions and associated detector noise will produce temperature and water vapor profiles with allowable RMS errors. This task is scheduled to commence immediately upon the receipt of the calibrated level 1B MAS data and once final refinements of the cloud mask algorithm are complete to the satisfaction of the MODIS science team.

Evaluation of "cloud clearing" algorithms such as the N* method will be assessed using simulation to help clearly define the criteria of when such algorithms may be employed in cloud contaminated situations. Figure 28 depicts instances in which the cloud clearing method fails to produce near clear sky like radiance spectra.

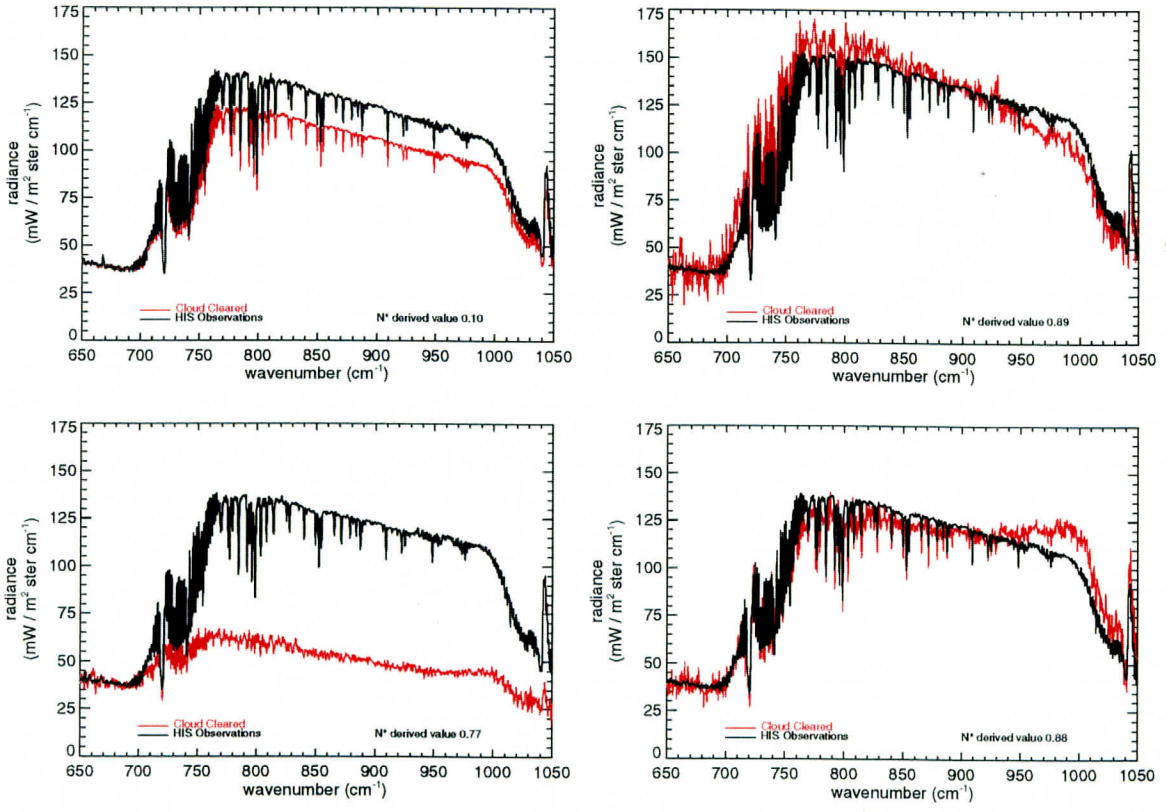

Figure 28. Four plots of the types of failures seen when applying the cloud clearing N* method. All simulated spatial resolutions using HIS data exhibit similar types of errors.

The types of failures in obtaining "cloud cleared" spectra are randomly present in all cases in which cloud clearing is evaluated as a function of spatial resolution. In order to address these shortcomings, this group intends to study the degree to which N* cloud clearing becomes unusable. A simulation will be performed in which temperature / water vapor profiles, cloud amount, cloud pressure levels, skin temperature, and surface emissivity are varied to show when breakdowns in N* start to occur. Such a

study is needed to clarify the criteria needed to successfully attempt cloud clearing, otherwise retrieval performance analysis of cloud cleared radiances may introduce conflicting data about trade-offs in cloud clearing as a function of spatial resolution and noise.

4.2 Future work for NAST scientific algorithm development

The NPOESS Atmospheric Sounding Testbed - Interferometer (NAST-I) is scheduled to fly on the NASA ER-2 during CAMEX III which is set for the Fall of 1998. Atmospheric products will be generated from commonly accepted retrieval algorithms which have been proven using HIS data. The spatial resolution of the data is to be at a full 2 km and the unapodized spectral resolution of 0.25 cm^{-1} will aid in assessing future sounder options. Simulation of lower spatial and spectral resolution of future sounders to be considered to fly onboard NPOESS can be accomplished with NAST-I data, and atmospheric products such as air and water vapor profiles, land and sea surface temperature emmissivities, land and sea surface temperatures, and cloud optical properties can be used to evaluate the impact of one instrument configuration versus another. The datasets provided by NAST-I will prove to be invaluable to the sounder community and the scientific community in large by defining future instruments which fulfill the scientific and operational goals to the fullest extent.

4.3 Future work in Field Program Support for NAST

The NAST instrument is set to fly on board the NASA ER-2 aircraft in several field programs during FY98. The initial checkout period or shakedown of the NAST instrument is scheduled for March of 1998, and a CIMSS instrument support team headed by Dr. Revercomb will provide technical assistance during these initial performance checkouts of the NAST instrument. The CIMSS instrument support team will also provide assistance during CAMEX-III; however, there is currently no direct support for UW scientists during this field campaign to perform data analysis or to provide useful instrument studies from the NAST instrument data sets obtained from upcoming field campaigns.

5.0 REFERENCES

Ackerman, S. A., K. I. Strabala, R. A. Frey, C. C. Moeller, and W. P. Menzel, 1996: Cloud mask for the MODIS Airborne Simulator (MAS): Preparation for MODIS. Presented at the Eighth Conference on satellite Meteorology and Oceanography., Jan 28 - Feb. 2, Atlanta, GA, AMS, 313-316.

Chahine, M. T., 1974: Remote sounding of cloudy atmospheres. I. The single cloud layer., *J. Atmos. Sci.*, **31**, 233-243.

Cousins, D., and W. L. Smith, 1997: National Polar Orbiting operational Environmental Satellite System (NPOESS) Airborne Sounder Testbed Interferometer (NAST-I).

Cuomo, V., C. Serio, V. Tramutoli, C. Pietrapertosa, F. Romano, 1992: Assessing the impact of higher spatial resolution on cloud filtering applied to infrared radiances. Universita dell Basilicata Rep., Basilicata, Italy.

Derrien, M., 1992: Influence of the size of field of view on contamination by clouds. Issue 0 contract report to EUMETSAT.

Huang, H. L., W. L. Smith, and M. S. Whipple, 1997: Information content analysis study of advanced sounders., Report to U.S. Department of Commerce, NOAA, Procurement Operations Division, Small Purchases Branch.

King, M. D., W. P. Menzel, P. S. Grant, J. S. Myers, G. T. Arnold, S. E. Platnick, L. E. Gumley, S. Tsay, C. C. Moeller, M. Fitzgerald, K. S. Brown, F. G. Osterwisch, 1996: Airborne scanning spectrometer for remote sensing of cloud aerosol, water vapor, and surface properties., *J. Atmo. Oceanic Technol.*, **13**, 777-794.

Rossow, W. B. and L. C. Garder, 1993: Cloud detection using satellite measurements of infrared and visible radiances for ISCCP. J. *Climate*, **6**, 2394-2418.

Smith, W. L., 1968: An improved method for calculating tropospheric temperature and moisture profiles from satellite radiometer measurements. *Monthly Weather Review*, **96**, 387-396.

Smith, W. L. and H. L. Huang, 1996: An advanced sounder cloud contamination study. *J. Appl Met.*, 35, **8**, 1249-1255